The flow of fresh groundwater and solutes to the world's oceans and coastal ecosystems

Elco Luijendijk[1*], Tom Gleeson[2], Nils Moosdorf[3]

[1] Geoscience center, University of Göttingen, Goldschmidstrasse 3, 37077, Göttingen, Germany, elco.luijendijk@geo.uni-goettingen.de

[2] Department of Civil Engineering and School of Earth and Ocean Sciences, University of Victoria, Victoria, British Columbia, Canada

[3] Leibniz Centre for Tropical Marine Research (ZMT), Bremen, Germany

*e-mail: elco.luijendijk@geo.uni-goettingen.de

Abstract:

The flow of fresh groundwater towards the world oceans may provide substantial inputs of critical nutrients and solutes to the oceans. Here we present the first spatially resolved global model of coastal groundwater discharge to show that, in contrast to most previous estimates, the contribution of fresh groundwater accounts for only 0.2% of the freshwater input and 1% of the solute input to the oceans. However, the coastal discharge of fresh groundwater displays a high spatial variability and for an estimated 20% of the world's estuaries, salt marshes and coral reefs the flux of terrestrial groundwater is high enough to pose a are at risk for pollution and eutrophication. Coastal groundwater discharge constitutes a diffuse and largely unmonitored source of nutrients which given the slow rates of groundwater flow may continue to pose a pollution risk for vulnerable coastal ecosystems long after sources of pollution have been addressed.

Submarine groundwater discharge, the flow of fresh or saline groundwater to oceans, may be a significant contributor to the water and chemical budgets of the world's oceans[1,2]. The fresh component of submarine groundwater discharge is critical due to its high solute and nutrient load[3], has been estimated to be up to 10% of the river discharge to the world's oceans[1] and to equal the inputs by rivers to the for solutes such as carbon[4], iron[5], silica[6,7] and strontium[8], and potentially buffers ocean acidification with groundwater alkalinity[9]. Although a large number of studies have estimated fresh submarine groundwater discharge (fresh SGD) locally, it is difficult to derive a global estimate from these point estimates, because they are highly variable, often uncertain and strongly biased towards high discharges[1]. Global-scale estimates of fresh SGD vary by four orders of magnitude, with the most recent estimates ranging up to 10% of the river discharge towards the oceans[1,2,10]. Large-scale spatially distributed estimates have only been published for the entire[11] or parts of the US coast[12]. The total flux of groundwater to the ocean (herein called coastal groundwater discharge) can be divided into three distinct fluxes (Fig. 1a): 1) fresh SGD that we consider to be meteoric groundwater discharging below the mean sea level; 2) near-shore terrestrial groundwater discharge (NGD) that is fresh groundwater discharging above the mean sea level in the first hundreds of meters near the coastline; and 3) recirculated sea water. Fresh SGD and NGD are driven by recharge from onshore precipitation and are critical due to their high solute and nutrient load whereas recirculated sea water is driven by waves, tides, storm surges and density-dependent flow. We use density-dependent groundwater models to quantify the partitioning of onshore and offshore groundwater discharge and the sensitivity of coastal discharge to controlling variables such as topography, permeability, recharge and size of coastal watersheds. We subsequently quantify coastal groundwater discharge at a global scale by combining a series of numerical models of coastal groundwater flow with a global geospatial analysis of controlling variables. In addition to submarine groundwater discharge we quantify near-shore terrestrial discharge, a flux that has been overlooked in most hydrological studies but affects coastal water budgets, evapotranspiration and ecosystems.

Controls on coastal groundwater discharge

Sensitivity analysis using a density-dependent model of coastal groundwater flow shows that fresh SGD is an insignificant part of the total groundwater flux in most coastal groundwater systems, and most groundwater discharges on land (Fig. 1d-g) where it contributes to baseflow to rivers and evapotranspiration. For a coastal groundwater system consisting of relatively permeable rocks (Fig. 1b) 29 % of the total groundwater recharged on land discharges in the oceans. However, for a system with the global median values of permeability and topographic gradient which were derived from a global geospatial analysis of coastal watersheds (see supplementary information section S1) the modeled fresh SGD flux is only 0.5% of the total recharge flux. The discharge flux reaches a maximum

of 0.23 m a^{-1} at the coastline (Supplementary Fig. S13), which is lower than the lowest local value of fresh SGD reported in the literature known to us[13]. While fresh SGD is insignificant in most cases, when permeability exceeds a threshold value of 10^{-12} m^2 and topographic gradients exceed 1%, fresh SGD increases rapidly and can become the dominant groundwater discharge component (Fig. 1e and 1g). Somewhat counterintuitively, groundwater recharge and size of the contributing area do not influence SGD in most cases. Once a threshold value is reached where groundwater input equals the flow capacity of the subsurface any further increases in recharge or contributing area only generate additional terrestrial discharge, whereas fresh SGD stays constant (Fig. 1d and 1f).

The model results show that offshore freshwater discharge is mirrored by a zone of near-shore terrestrial groundwater discharge (NGD) (Fig. 1b), which is higher than fresh SGD in most settings except at high permeability or topographic gradients (Fig. 1d-g), but has to our knowledge been overlooked in global hydrological assessments. The existence of onshore groundwater seepage near surface water features has long been recognized for lakes, wetland or streams[14,15]. However, seepage near coastlines has not been quantified at large scales. In the two-dimensional cross-sectional models presented here near-shore discharge generates a seepage flux across the land surface that peaks at the coastline and decays exponentially with distance to the coast (Fig. 1b and SI Fig. S13). This modeled seepage flux represents a mixture of evapotranspiration, ponding, surface runoff and lateral groundwater flow perpendicular to the cross-section towards streams.
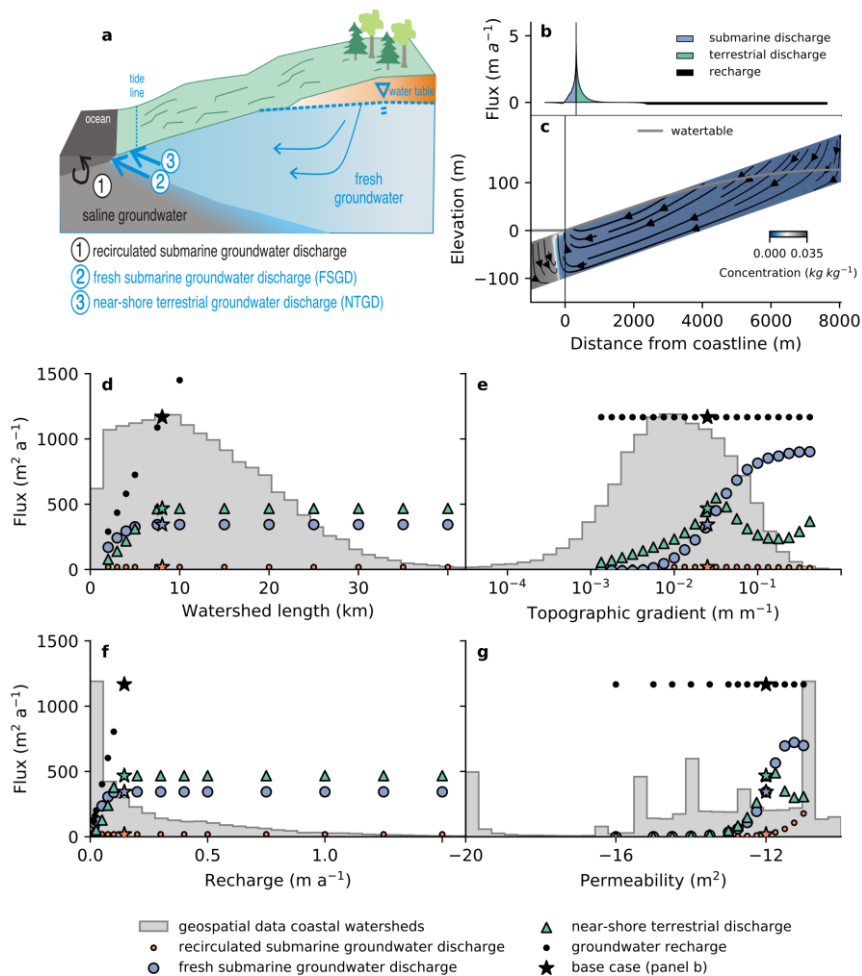
Fig. 1. Sensitivity analysis (d-g) of numerical models of coastal groundwater discharge (a-b) demonstrates that the flux of groundwater to the ocean is controlled primarily by topographic gradient (e) and aquifer permeability (g) and is relatively insensitive to watershed length (d) and groundwater recharge (f). The histograms in panels d-f show the distribution of the controlling parameters in all 40,082 global coastal watersheds. Panel b and c show modeled groundwater fluxes over the land surface and seabed (b), flowlines and salinity (c) for a base-case model coastal watershed with global median values for groundwater recharge (0.143 m a^{-1}), but with relatively high permeability (10^{-12} m^2) and topographic gradient (2.5%).

Global coastal groundwater discharge

Due to the relatively small area of coastal watersheds, even if all groundwater recharge in coastal watersheds were to discharge directly into the oceans, fresh SGD would not exceed 5.5% of the river input into the world's oceans. Although groundwater flow does not necessarily follow surface watershed boundaries, sensitivity analysis shows that coastal groundwater discharge is relatively insensitive to the size of the contributing area and is instead in most cases limited by the flow capacity of coastal aquifers, which is a function of their permeability, thickness and topographic gradient (Fig. 1d). The exceptions are models with relatively high permeability (>~10^{-12} m^2) and high topographic gradient (>~1%), which however constitute a small part of the global coastal watersheds.

Global coastal groundwater discharge, fresh SGD and NGD were calculated by pairing the results of 351 model runs to geospatial data of 40,082 coastal watersheds (Fig. 2, S8 and S9). The results show that fresh SGD is an insignificant contributor to the water and solute budgets of the world's oceans (Supplementary Fig. S8). Only 4 (0.04-11) % of the groundwater recharged in coastal watersheds is discharged offshore. The calculated global fresh submarine groundwater discharge is 78 (0.4-210) km^3 a^{-1}, which amounts to 0.2 (0.001 − 0.6)% of the river discharge to the oceans[16] and which is at the lower end of previous global estimates[1,10]. The uncertainty of the global fresh SGD flux is mostly caused by the high uncertainty of the values of permeability that were used. Additional sources of uncertainty are the representative topographic gradient of coastal watersheds, groundwater recharge and the size the area that contributes to fresh SGD. Fresh SGD would be 44 instead of 78 km^3 a^{-1} when a lower estimate of topographic gradients would be adopted that follows the average gradient of coastal streams instead of the average gradient. The difference between two alternative global models of groundwater recharge results in an uncertainty range of 53 to 78 km^3 a^{-1}. When the contributing area is assumed to be twice the size of coastal watersheds the fresh SGD flux is 118 km^3 a^{-1}. While the uncertainty ranges reported here are large, the best estimates of permeability, topographic gradient and recharge provide a good fit of the model to observed watertable gradients in coastal watersheds (Supplementary Fig. S11), which suggests that the reported best estimates of coastal discharge fluxes are relatively robust.

The calculated fresh SGD is only a minor fraction, 0.06% (0.0003% - 0.2%), of the global total SGD flux, which includes recirculated seawater, and has been estimated as three to four times of the river flux globally based on measured concentrations of radiogenic radon in seawater[17]. This is in line with analytical models that estimated seawater circulation due to tidal and wave forcing to be roughly equal to the estimated total SGD flux[18]. The very low terrestrial contribution to the overall SGD flux means that global SGD consists almost exclusively of recirculated seawater and the net-input of solutes to the oceans by SGD is much lower than previously assumed. A first order estimate of the input by fresh SGD of carbon, nitrogen, silica and strontium based on published compilations of the average solute concentrations in coastal groundwater[7,8,19,20] suggest the contribution of submarine groundwater discharge is ~1% of the input by rivers (Table 1), which is much smaller than the up to 100% contribution suggested by some recent studies that extrapolated global inputs from local and regional-scale estimates[4–6]. There are insufficient data available for the concentration of iron in coastal groundwater, but even with relatively high concentrations of 40 mg L^{-1} that exceed local estimates in the literature[5] the contribution would equal 1% of the river flux[21]. Our estimate of solute fluxes in fresh SGD is a first order, spatially aggregated average that assumes conservative transport. The spatially distributed map of coastal groundwater discharge (Fig. 3) provides the

possibility of better future estimates for locations where concentrations of specific solutes are known.

In addition to submarine groundwater discharge, the model results suggest that a substantial part of coastal groundwater discharge takes place onshore (Supplementary Fig. S9). Global NGD is estimated as 147 (1 - 289) km^3 a^{-1}, which is 0.4 (0.001-0.8) % of the global river discharge. NGD takes place in a zone that on average extends 400 m from the shore (Supplementary Fig. S15). NGD predominantly contributes to evapotranspiration, but exceeds potential evapotranspiration[22] in 28 (0.07-58) % of the global coastline where it contributes to surface runoff and baseflow close to the shoreline. The combined submarine and near-shore groundwater discharge flux equals 224 (1.4 − 500) km^3 a^{-1} and is shown in Fig. 3a. Model experiments demonstrate that the partitioning of coastal groundwater discharge in submarine and terrestrial discharge is highly sensitive to the local topographic gradient (Fig. 1d), and therefore the total coastal groundwater discharge is a more robust estimate than the onshore and offshore components.
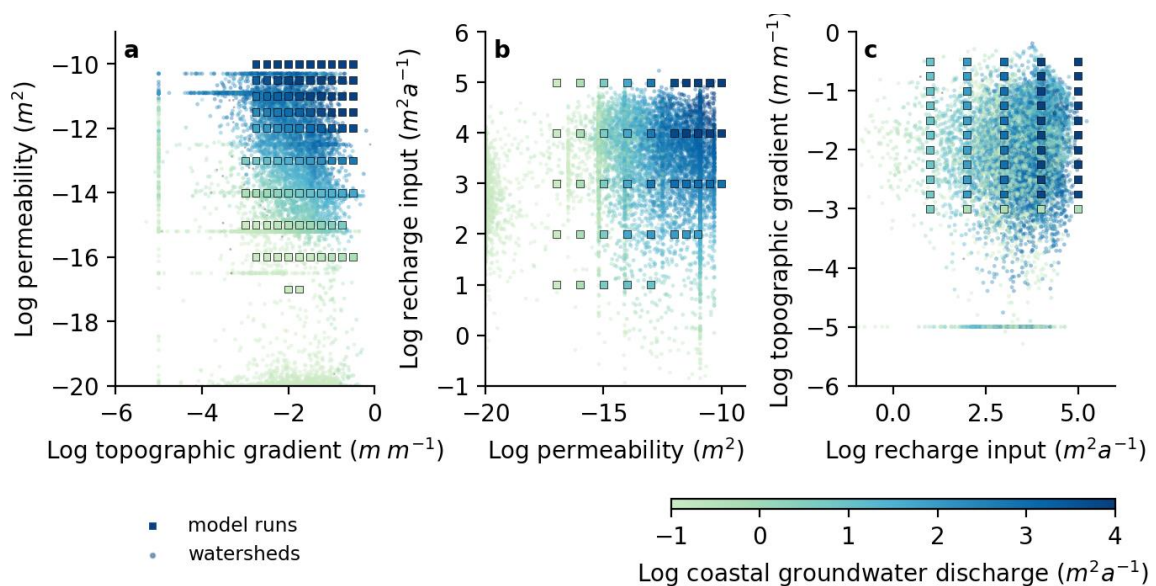

Fig. 2. Interpolation of coastal groundwater discharge for each of the 40082 global coastal watersheds from a series of 351 model runs that cover the range of permeability, topographic gradients and groundwater recharge found in these watersheds. Note that in each panel the model runs are shown with the highest modeled coastal groundwater discharge. For instance, for panel a behind each square there are a number of model runs that are not shown with different recharge input values.
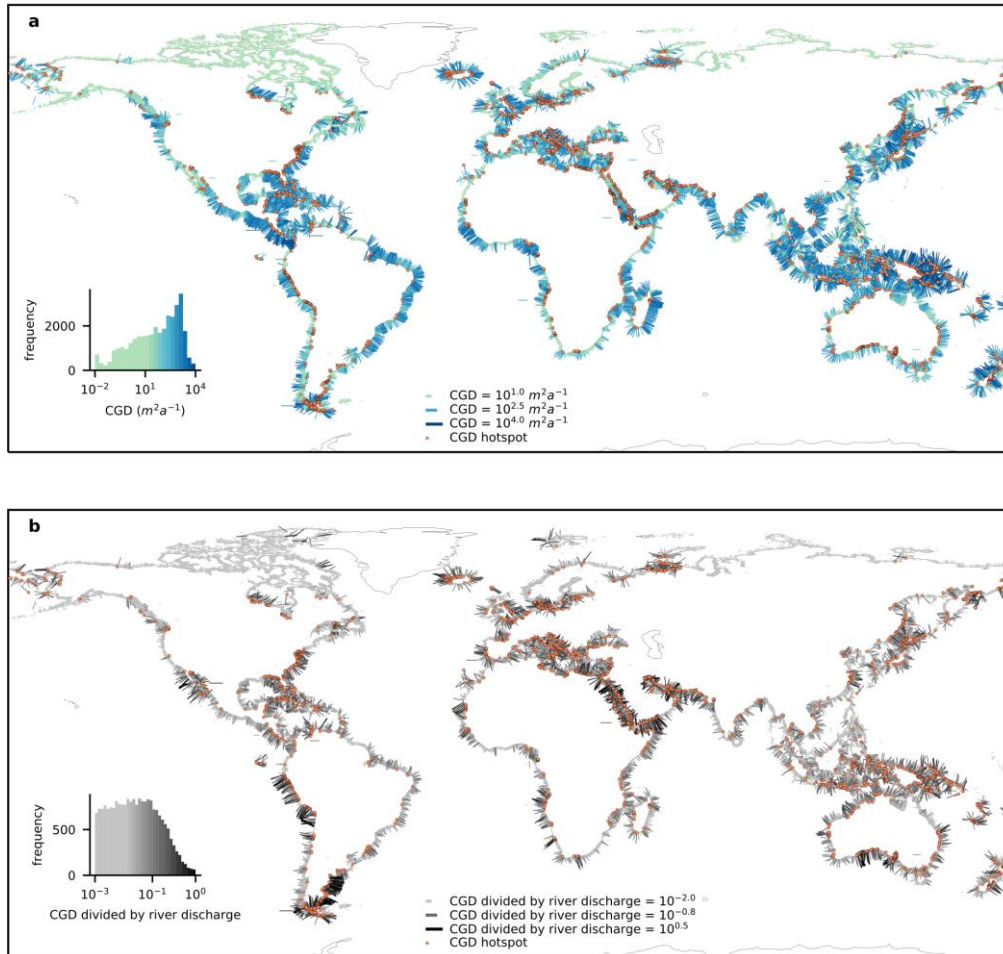
Fig. 3. The flow of groundwater to the oceans is highly variable, dominated by localized hotspots, and can locally be source of water that rivals surface water discharge. Global maps of a) coastal groundwater discharge (CGD) in m^2 a^{-1} and b) coastal groundwater discharge (CGD) divided by the surface water flux to the oceans.

Table 1. Comparison of the calculated solute flux to the oceans by rivers and fresh submarine groundwater discharge shows that the contribution of fresh groundwater is much lower than previously assumed. The calculated flux is based on the modeled submarine groundwater discharge and previously reported values of the average concentrations of solutes in coastal groundwater systems.

Solute	River flux	Previous estimate fresh SGD	Average concentration in fresh SGD	New estimate fresh SGD	References
	$(kg\ a^{-1})$	(% of river flux)	$(mg\ L^{-1})$	(% of river flux)	
Dissolved inorganic carbon	7.1 (6.5-7.7) $\times 10^{11}$	23% (17%-39%)	60	0.7% (0.003%-1.9%)	[63]

Dissolved inorganic nitrogen	1.9×10^{10}	7.5%	2	0.8% (0.004%-2.2%)	[19,20,64,66]
Dissolved silica	1.7×10^{11}	8%	8 (6-11)	0.5% (0.001%-2.1%)	[7,67]
Strontium	2.9 (1.6-4.1) $\times 10^{9}$	21% (15%-149%)	0.25	0.7% (0.002-3.3%)	[8]

Hotspots of coastal groundwater discharge

Although the overall contribution of water and solutes by coastal groundwater discharge to the oceans is low, coastal groundwater discharge is highly variable, with 10% of the global coastline contributing 90% of the total discharge. Comparison with data on the discharge of rivers to the oceans[23] shows that coastal groundwater discharge is highly variable and can locally be close to the river input (Fig. 3a and 3b), which given its relatively high solute load[3] means that it may dominate the solute input in some coastal ecosystems. We define coastal groundwater discharge hotspots as watersheds where the coastal groundwater discharge exceeds 100 m^2 a^{-1} and 25% of the river discharge. The threshold value of 100 m^2 a^{-1} reflects a relatively conservative lower bound for reported values at locations with high coastal groundwater discharge (Supplementary Tables S5, S6) and associated ecosystem impacts (Supplementary Table S7). Coastal groundwater discharge hotspots (Fig. 3a and 3b) cover 9 (0.02-30) % of the global coastline and are predominantly located in areas with a steep coastal topography due to glacio-isostatic rebound, active tectonics or volcanic activity and areas consisting permeable unconsolidated sediments, carbonates or volcanic rocks (Supplementary Fig. S16). The distribution of hotspots is consistent with documented sites of high fresh groundwater discharge globally that are predominantly located in North America, Europe and East Asia (Supplementary Table S6 and S7). However, at many hotspots, such as Iceland and parts of South America, Africa and south Asia, and many tropical islands coastal groundwater discharge has been unexplored to our knowledge.

Local impacts of coastal groundwater discharge

Due to its high spatial variability, fresh groundwater discharge can locally have strong impacts on coastal hydrology and ecosystems. Coastal groundwater discharge can control the salinity, nutrient

budget and productivity of coastal lagoons[24], salt marshes[25] and mangroves[26], and can cause eutrophication[27], algal blooms[28] and the degradation of coral reefs[29]. In particular, tropical islands consisting of volcanic and carbonate rocks are likely to host high fresh groundwater fluxes (Supplementary Fig. S16) that can supply crucial nutrients to marine ecosystems that may be located far from other nutrient sources[30]. A first order estimate of global coastal groundwater eutrophication risk (Fig. 4a) shows that 13% (0.2-23%) of the global coastline is at risk of eutrophication by terrestrially derived groundwater and nutrients. Eutrophication risk is defined by nitrogen application in coastal watersheds that exceeds 10 kg ha^{-1} and coastal discharge that exceeds 100 m^2 a^{-1}. The threshold value for nitrogen input corresponds to values that have historically led to strongly elevated nitrogen concentrations in groundwater in Europe and North America[31,32] that have contributed to the eutrophication of terrestrial and nearshore ecosystems[33]. Coastal areas with elevated risk include sensitive coastal ecosystems. A comparison with published locations of these ecosystems[34–36] shows that 26% (0.4%-39%) of the world's estuaries and 17% (0.3%-31%) of the salt marshes at risk of eutrophication. In addition, 14% (0.1-26%) of the coastline that is located within 500 m of a coral reef is at risk of eutrophication. A review of sites with documented ecosystem impacts of coastal groundwater discharge (Supplementary Table S7) suggests that the threshold values of coastal groundwater discharge and nitrogen input in the adjacent coastal watersheds that we used to define high risks are relatively conservative and that adverse ecosystem impacts may also occur at lower threshold values for nitrogen application or coastal groundwater discharge. In addition to its importance for coastal ecosystems, coastal groundwater discharge can locally also be a freshwater resource that is used as drinking water or for other purposes in a limited number of locations, but has been generally overlooked[37]. However, this resource may also be sensitive to pollution, and exploitation of this resource would need to be carefully managed to avoid salt-water intrusion and adverse impacts on coastal ecosystems.

The values of global coastal groundwater discharge represent a natural undisturbed system and do not include groundwater pumping. However, many coastal groundwater systems may be affected by groundwater pumping. A comparison of the calculated coastal groundwater flux and published values of groundwater depletion in coastal watersheds[38] shows that in most coastal groundwater systems are not associated with depletion (Fig. 4b). Groundwater depletion is concentrated in semi-arid regions and in 13% (8% - 19%) of the global coastal watersheds groundwater depletion exceeds coastal groundwater discharge. In these watersheds coastal groundwater discharge has already or will reduce to zero at some stage in the future and instead seawater will start intruding into terrestrial groundwater systems.
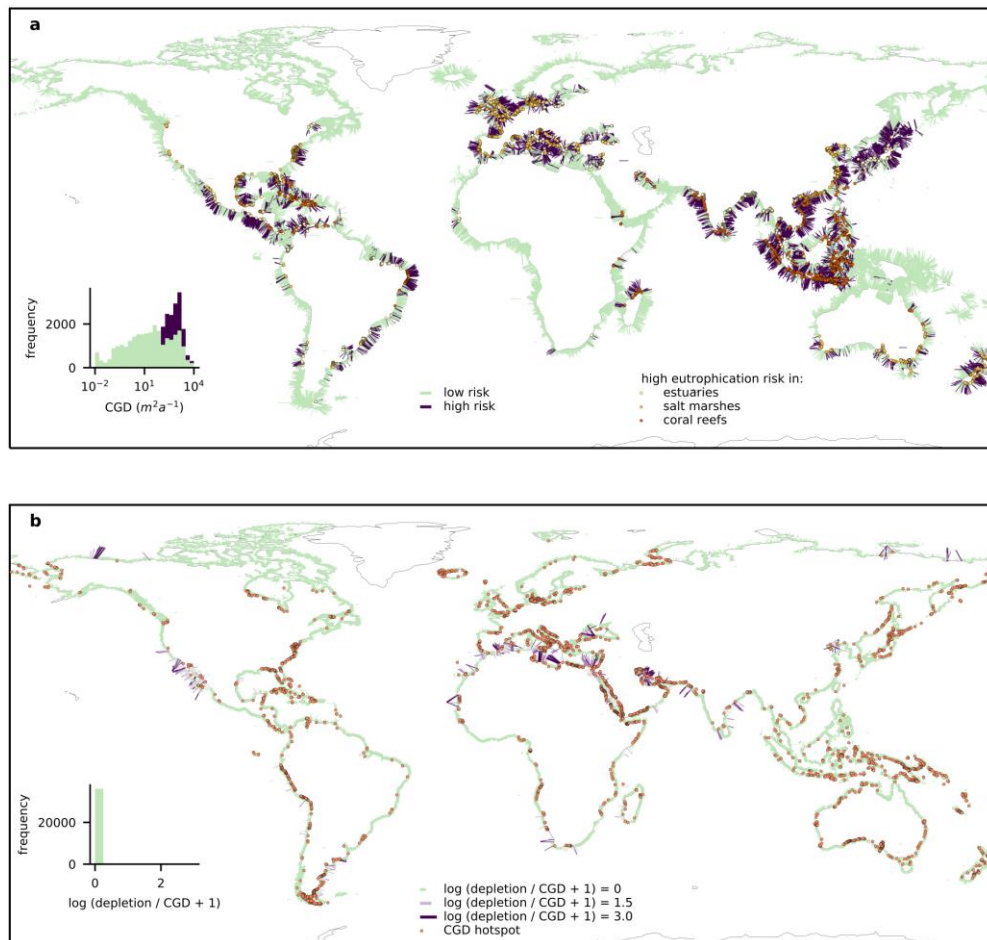
Fig. 4. Coastal groundwater discharge can locally pose a eutrophication and pollution risk to coastal ecosystems (panel a). Although the majority of coastal watersheds groundwater depletion is lower than coastal groundwater discharge, groundwater depletion locally exceeds coastal groundwater discharge in approximately 13% of the global coastline (panel b).

Comparison with published large-scale models of coastal groundwater discharge

Our model results estimate a coastal groundwater discharge flux for the contiguous US of 8.5 (0.1-17) km^3 a^{-1}, which is in the same range as the 15±4 km^3 a^{-1} estimated by Sawyer et al. [11]. However, the two estimates cannot be compared directly. The estimate by Sawyer et al. is based on the assumptions that groundwater discharge is controlled solely by surface morphology and drainage density, which is a debatable assumption. In contrast our model experiments highlight the role of the flow capacity of the subsurface and the key role of permeability in governing groundwater flow and discharge in coastal groundwater systems (Fig. 1 and 2). For the Gulf and Atlantic coasts of the USA our model estimates a coastal discharge of 6.6 (0.1-11.3) km^3 a^{-1}, which is at the lower end of recent estimates by Zhou et al.[39] that range from 9.7 (7.2-12.0) to 27.1 (22.8-30.5) km^3 a^{-1}. These estimates are based on a series of regional groundwater models[12], include more detailed hydrogeology and

permeability structure and may therefore be more accurate than our model estimates, especially at local scales. On the other hand, these models did not include solute transport and density-dependent flow and used a discretization of 250 m. As a result, the partitioning of groundwater discharge around the coastline may not have been well resolved, and not including the fresh-salt water interface may have led to overestimation of coastal groundwater discharge. Both methods are difficult to apply to global scales. Methods based on surface morphology and hydrography depend critically on the availability of high resolution datasets that are currently only available for part of the global coastline. While there have been recent advances towards global 3D groundwater models[40], the prohibitive computational expense of including density-riven flow in these models limits their utility for resolving coastal groundwater fluxes.

Conclusions

The assessment of near-shore submarine and terrestrial groundwater discharge reported here provides the first estimate at high spatial resolution of these water fluxes at a global scale. Our analysis shows that the global flux is dominated by a small number of coastal watersheds that are distributed around the globe, including numerous locations that have so far not been explored. In contrast to river discharge, coastal groundwater discharge is frequently unmonitored. However, our global analysis shows that locally coastal groundwater discharge can in many cases pose an equally serious risk for coastal water quality and coastal ecosystems. In addition, groundwater discharge is relatively diffuse compared to surface water discharge and may therefore affect larger areas. Coastal groundwater discharge links onshore groundwater systems with coastal ecosystems, which means that changes in groundwater pumping or land use affect the flow of nutrients to coastal ecosystems [41,42], and should be taken into account in coastal environmental management. The estimates provided here can help guide future research and monitoring of this water flux and its effect on coastal ecosystems. This is especially important as population pressures and increase in agricultural activity are likely to increase nutrient and contaminant inputs to coastal groundwater in many areas in the future. Furthermore, because groundwater flow rates are typically very slow, measures to improve groundwater quality onshore may take decades before they affect offshore water quality[43]. Therefore, quantitative estimates of coastal groundwater discharge are of key importance for identifying present and future risks to coastal water quality.

Methods

Modeling coastal groundwater discharge

We simulated submarine and terrestrial groundwater discharge in coastal groundwater systems

using a numerical model of coupled density-driven groundwater flow and solute transport. The model code, GroMPy-couple, is a Python shell around the finite element code escript[44,45] which has been used to simulate subsurface fluid flow[44]. We implemented an iterative scheme[46] to solve the fluid flow and solute transport equations and the equations of state for fluid density and viscosity. GroMPy-couple uses an implementation of a seepage boundary condition based on an existing implementation in the model code MODFLOW[15], which ensures a realistic and numerically stable partitioning between onshore and offshore groundwater discharge in models of coastal groundwater systems[15]. The model code simulates the flow of fresh (meteoric) groundwater, the mixing and recirculation of seawater at the fresh-salt water interface at the coast due to dispersion and the onshore and offshore discharge of groundwater. We did not model transient processes like tidal forcing of groundwater flow and wave setup, that are responsible for the bulk of the recirculation of seawater in coastal aquifers[47,48]. Note that the submarine discharge of fresh groundwater is relatively insensitive to transient seawater circulation offshore[48]. The model code has been validated by comparison with a salt water intrusion experiment[49], analytical solutions of groundwater discharge[14,15], and model experiments using the widely-used model code SUTRA[50]. See Supplementary Information section S2 for more details of the model approach.

Geospatial data analysis

The model input was based on a geospatial data analysis of the controlling parameters of coastal groundwater discharge. We analyzed watershed geometry[51], topographic gradients[52], permeability[53,54] and groundwater recharge[23,55] for 40082 coastal watersheds globally (see Supplementary Figure 1). We use coastal watersheds as a first order estimate of the spatial scale of coastal groundwater flow systems. While watersheds may be a good first order approximation of the contributing area for coastal groundwater systems, model experiments[56] and water budget analysis of river basins[57] indicate that there may be a significant component of regional groundwater flow that crosses watershed boundaries in some systems. To account for this we used a contributing area that is two times the size of coastal watersheds as an upper estimate for the calculation of coastal groundwater discharge, which covers the upper end of reported percentages of regional flow in previous work[56,57]. We use a modified version of the global permeability map[53,54] where higher values of permeability were assigned to the predominantly karstic coastal carbonates and unconsolidated sediments, which are frequently dominated by coarse deposits in coastal settings (see Supplementary Information section S2). Topographic gradients were calculated by dividing the elevation by the distance to the coastline. Two alternatives for the representative gradient were used that included the average gradient of all points in a coastal watershed and the gradient of points that coincided with a stream only.

Global coastal groundwater discharge fluxes

Global fluxes of fresh SGD and terrestrial discharge were obtained by linear interpolation of 357 model results to the 40082 coastal watersheds (see Supplementary Fig. S8 and S9). The interpolation is based on a comparison of permeability, topographic gradient and recharge input, which is the product of groundwater recharge and the size of the contributing area, for the model results and the geospatial data of coastal watersheds. We used reported ±1 standard deviation uncertainty of permeability[54], the differences between two alternative recharge datasets[23,55] and the differences in the topographic gradients between elevation grid nodes covered by streams and the entire coastal watershed to calculate minimum and maximum estimates of the discharge fluxes. The interpolated discharge values were compared to published values of surface runoff[23], potential evapotranspiration[22] and tide and storm surge elevation[58], which were assigned to each watershed using GIS tools.

Model-data comparison

Comparison between modeled and measured hydraulic gradients in 336 coastal watersheds with water level observations from a global dataset[59] shows that the ratio of the modeled values over the measured values is 1.08 (see Supplementary section S6 and Fig. S11) when using the best estimates of permeability, recharge and topographic gradients. This shows that the model provides a realistic estimate of coastal groundwater flow. Overall ~60% of the local variability in water table gradient is captured. The remaining scatter is likely due to the large spatial scale of our models (on average 11 km) and the limitations of the global datasets supporting our analysis. A qualitative comparison with locations of reported ecosystem impacts by fresh SGD and reported use of fresh SGD shows that in all of these locations the modeled fresh SGD is much higher than the median of all coastal watersheds globally (see Supplementary Table S6 and S7). Comparison to a selection of ten published local estimates of fresh SGD shows that for five studies the modeled and reported fresh SGD values fit within uncertainty bounds (Supplementary Fig. S12a and Table S7). However, for the remaining locations the reported values strongly exceed the modeled values, but the reported fresh SGD also exceeds the total groundwater recharge in adjacent coastal watersheds (Supplementary Fig. S12b), which suggests that these studies strongly overestimate fresh SGD. The frequent inconsistency of fresh SGD estimates with onshore groundwater budgets has been noted by several earlier authors[11,60] and may be due to uncertainties in methods to quantify fresh water discharge[61,62] or biased selection and reporting of study sites for SGD[1].

Quantifying solute transport, eutrophication risk and groundwater depletion

First-order estimates of the global solute flux that is transported by fresh SGD were calculated by multiplying the calculated global fresh SGD flux with previously reported average values for the concentrations of nitrogen[19,20], carbon[63], silica[7] and strontium[8] in coastal groundwater. These estimates were compared to published values of the solute flux by surface runoff and earlier estimates of the contribution of fresh SGD[7,8,63,64]. See supplementary section S4 for a more detailed discussion of these data sources. Note that our estimates assume conservative transport and do not take into account fluid-rock interaction and microbial activity in coastal aquifers. The risk of eutrophication of coastal ecosystems was estimated by comparing locations of high groundwater discharge with high agricultural nitrogen inputs in coastal watersheds. Areas with high risk were identified if discharge exceeded a threshold of 100 m^2 a^{-1} and nitrogen inputs[65] exceed 10 kg ha^{-1}. The threshold value for nitrogen input corresponds to values that have historically led to strongly elevated nitrogen concentrations in groundwater in Europe and North America[31,32] that have contributed to the eutrophication of terrestrial and nearshore ecosystems[33]. We compared the modeled coastal discharge fluxes to groundwater depletion by using published groundwater depletion rates[38] and multiplying these rates with the area of coastal watersheds.

Author contributions

TG conceived this study. EL and TG designed the methods. EL constructed the model code and conducted the geospatial analysis and numerical modeling. All authors contributed to interpretation and discussion of the results and writing the manuscript.

Data availability

The results of the model sensitivity analysis and the parameter space exploration are available as supplementary data files S1 and S2, respectively. The results of the geospatial analysis and the interpolated coastal groundwater discharge fluxes for the global watersheds are available in shapefile format as supplementary data file S3. The data files are also available on Pangea (url to be supplied).

Code Availability

The model code used to simulate coastal groundwater discharge (GroMPy-couple) is available at GitHub (https://github.com/ElcoLuijendijk/GroMPy-couple), along with the parameter files required to replicate the results of this study. The code has also been published at Zenodo[68].

References

1. Taniguchi, M., Burnett, W. C., Cable, J. E. & Turner, J. V. Investigation of submarine groundwater discharge. *Hydrol. Process.* **16**, 2115–2129 (2002).

2. Moore, W. S. The Effect of Submarine Groundwater Discharge on the Ocean. *Ann. Rev. Mar. Sci.* **2**, 59–88 (2010).

3. Slomp, C. P. & Van Cappellen, P. Nutrient inputs to the coastal ocean through submarine groundwater discharge: Controls and potential impact. *J. Hydrol.* **295**, 64–86 (2004).

4. Liu, Q. *et al.* Effect of submarine groundwater discharge on the coastal ocean inorganic carbon cycle. *Limnol. Oceanogr.* **59**, 1529–1554 (2014).

5. Windom, H. L., Moore, W. S., Niencheski, L. F. H. & Jahnke, R. A. Submarine groundwater discharge: A large, previously unrecognized source of dissolved iron to the South Atlantic Ocean. *Mar. Chem.* **102**, 252–266 (2006).

6. Kim, G., Ryu, J.-W., Yang, H.-S. & Yun, S.-T. Submarine groundwater discharge (SGD) into the Yellow Sea revealed by 228Ra and 226Ra isotopes: Implications for global silicate fluxes. *Earth Planet. Sci. Lett.* **237**, 156–166 (2005).

7. Tréguer, P. J. & De La Rocha, C. L. The world ocean silica cycle. *Ann. Rev. Mar. Sci.* **5**, 477–501 (2013).

8. Beck, A. J., Charette, M. A., Cochran, J. K., Gonneea, M. E. & Peucker-Ehrenbrink, B. Dissolved strontium in the subterranean estuary - Implications for the marine strontium isotope budget. *Geochim. Cosmochim. Acta* **117**, 33–52 (2013).

9. Cyronak, T., Santos, I. R., Erler, D. V. & Eyre, B. D. Groundwater and porewater as major sources of alkalinity to a fringing coral reef lagoon (Muri Lagoon, Cook Islands).

Biogeosciences **10**, 2467–2480 (2013).

10.   Taniguchi, M., Ishitobi, T., William Burnett, C. & Shimada, J. Comprehensive evaluation of the groundwater-seawater interface and submarine groundwater discharge. *IAHS-AISH Publ.* 86–92 (2007).

11.   Sawyer, A. H., David, C. H. & Famiglietti, J. S. Continental patterns of submarine groundwater discharge reveal coastal vulnerabilities. *Science (80-.).* **10**, 705–708 (2016).

12.   Befus, K. M., Kroeger, K. D., Smith, C. G. & Swarzenski, P. W. The Magnitude and Origin of Groundwater Discharge to Eastern U.S. and Gulf of Mexico Coastal Waters. *Geophys. Res. Lett.* 396–406 (2017). doi:10.1002/2017GL075238

13.   Reay, W. G., Gallagher, D. L. & Simmons, G. M. groundwater discharge and its impact on surface water quality in a Chesapeake Bay inlet. *JAWRA J. Am. Water Resour. Assoc.* **28**, 1121–1134 (1992).

14.   Bokuniewicz, H. J. Analytical Descriptions of Subaqueous Groundwater Seepage. *Estuaries* **15**, 458 (1992).

15.   Batelaan, O. & De Smedt, F. SEEPAGE, a new MODFLOW DRAIN package. *Ground Water* **42**, 576–88 (2004).

16.   Fekete, B. M., Vörösmarty, C. J. & Grabs, W. High-resolution fields of global runoff combining observed river discharge and simulated water balances. *Global Biogeochem. Cycles* **16**, (2002).

17.   Kwon, E. Y. *et al.* Global estimate of submarine groundwater discharge based on an observationally constrained radium isotope model. *Geophys. Res. Lett.* **41**, 8438–8444 (2014).

18.   Riedl, R. J., Huang, N. & Machan, R. The subtidal pump: a mechanism of interstitial water exchange by wave action. *Mar. Biol.* **13**, 210–221 (1972).

19.   Panno, S. V, Kelly, W. R., Martinsek, A. T. & Hackley, K. C. Estimating Background and Threshold Nitrate Concentrations Using Probability Graphs. *Ground Water* **44**, 697–709 (2006).

20.   Mueller, D. K. & Helsel, D. R. *Nutrients in the Nation's Waters--Too Much of a Good Thing? U.S. Geological Survey Circular* **1136**, (1996).

21.   Poulton, S. W. & Raiswell, R. The low-temperature geochemical cycle of iron: From continental fluxes to marine sediment deposition. *Am. J. Sci.* **302**, 774–805 (2002).

22.   Trabucco, A. & Zomer, R. J. Global aridity index (global-aridity) and global potential evapo-transpiration (global-PET) geospatial database. *CGIAR Consortium for Spatial Information* (2009).

23.   De Graaf, I. E. M., Sutanudjaja, E. H., Van Beek, L. P. H. & Bierkens, M. F. P. A high-resolution global-scale groundwater model. *Hydrol. Earth Syst. Sci.* **19**, 823–837 (2015).

24.   Johannes, R. E. & Hearn, C. J. The effect of submarine groundwater discharge on nutrient and

salinity regimes in a coastal lagoon off Perth, Western Australia. *Estuar. Coast. Shelf Sci.* **21**, 789–800 (1985).

25.   Krest, J. M., Moore, W. S., Gardner, L. R. & Morris, J. T. Marsh nutrient export supplied by groundwater discharge: Evidence from radium measurements. *Global Biogeochem. Cycles* **14**, 167–176 (2000).

26.   Maher, D. T., Santos, I. R., Golsby-Smith, L., Gleeson, J. & Eyre, B. D. Groundwater-derived dissolved inorganic and organic carbon exports from a mangrove tidal creek: The missing mangrove carbon sink? *Limnol. Oceanogr.* **58**, 475–488 (2013).

27.   Hwang, D.-W., Lee, Y.-W. & Kim, G. Large submarine groundwater discharge and benthic eutrophication in Bangdu Bay on volcanic Jeju Island, Korea. *Limnol. Oceanogr.* **50**, 1393–1403 (2005).

28.   Hu, C., Muller-Karger, F. E. & Swarzenski, P. W. Hurricanes, submarine groundwater discharge, and Florida's red tides. *Geophys. Res. Lett.* **33**, (2006).

29.   Paytan, A. *et al.* Submarine groundwater discharge: An important source of new inorganic nitrogen to coral reef ecosystems. *Limnol. Oceanogr.* **51**, 343–348 (2006).

30.   Kim, G., Kim, J.-S. & Hwang, D.-W. Submarine groundwater discharge from oceanic islands standing in oligotrophic oceans: Implications for global biological production and organic carbon fluxes. *Limnol. Oceanogr.* **56**, 673–682 (2011).

31.   Ascott, M. J. *et al.* Global patterns of nitrate storage in the vadose zone. *Nat. Commun.* **8**, 1416 (2017).

32.   Hansen, B., Thorling, L., Schullehner, J., Termansen, M. & Dalgaard, T. Groundwater nitrate response to sustainable nitrogen management. *Sci. Rep.* **7**, 1–12 (2017).

33.   Vitousek, P. M. *et al.* Human alteration of the global nitrogen cycle: Source and consequences. *Ecol Appl* **7**, 737–750 (1997).

34.   Alder, J. Putting the coast in the 'Sea Around Us'. *Sea Around Us Newsl.* **15**, 1–2 (2003).

35.   Mcowen, C. J. *et al.* A global map of saltmarshes. *Biodivers. Data J.* **5**, e11764 (2017).

36.   UNEP-WCMC, WorldFish Centre, WRI & TNC. Global distribution of warm-water coral reefs, compiled from multiple sources including the Millennium Coral Reef Mapping Project. Version 1.3. (2010).

37.   Moosdorf, N. & Oehler, T. Societal use of fresh submarine groundwater discharge: An overlooked water resource. *Earth-Science Rev.* **171**, 338–348 (2017).

38.   Wada, Y. *et al.* Global depletion of groundwater resources. *Geophys. Res. Lett.* **37**, 1–5 (2010).

39.   Zhou, Y. Q., Befus, K. M., Sawyer, A. H. & David, C. H. Opportunities and Challenges in Computing Fresh Groundwater Discharge to Continental Coastlines: A Multimodel Comparison for the United States Gulf and Atlantic Coasts. *Water Resour. Res.* **54**, 8363–8380

(2018).

40. de Graaf, I. E. M. *et al.* A global-scale two-layer transient groundwater model: Development and application to groundwater depletion. *Adv. Water Resour.* **102**, 53–67 (2017).

41. Crotwell, A. M. & Moore, W. S. Nutrient and Radium Fluxes from Submarine Groundwater Discharge to Port Royal Sound, South Carolina. *Aquat. Geochemistry* **9**, 191–208 (2003).

42. Knee, K. L., Street, J. H., Grossman, E. E., Boehm, A. B. & Paytan, A. Nutrient inputs to the coastal ocean from submarine groundwater discharge in a groundwater-dominated system: Relation to land use (Kona coast, Hawaii, U.S.A.). *Limnol. Oceanogr.* **55**, 1105–1122 (2010).

43. Tait, D. R. *et al.* The influence of groundwater inputs and age on nutrient dynamics in a coral reef lagoon. *Mar. Chem.* **166**, 36–47 (2014).

44. Poulet, T., Gross, L., Georgiev, D. & Cleverley, J. escript-RT: Reactive transport simulation in Python using escript. *Comput. \& Geosci.* **45**, 168–176 (2012).

45. Gross, L., Bourgouin, L., Hale, A. J. & Muhlhaus, H.-B. Interface Modeling in Incompressible Media using Level Sets in Escript. *Phys. Earth Planet. Inter.* **163**, 23–34 (2007).

46. Ackerer, P. A new coupling algorithm for density-driven flow in porous media. *Geophys. Res. Lett.* **31**, L12506 (2004).

47. Santos, I. R., Eyre, B. D. & Huettel, M. The driving forces of porewater and groundwater flow in permeable coastal sediments: A review. *Estuar. Coast. Shelf Sci.* **98**, 1–15 (2012).

48. Li, L., Barry, D. A., Stagnitti, F. & Parlange, J. Y. Submarine groundwater discharge and associated chemical input to a coastal sea. *Water Resour. Res.* **35**, 3253–3259 (1999).

49. Goswami, R. R. & Clement, T. P. Laboratory-scale investigation of saltwater intrusion dynamics. *Water Resour. Res.* **43**, n/a-n/a (2007).

50. Voss, C. I. & Provost, A. M. *SUTRA, A model for saturated-unsaturated variable-density ground-water flow with solute or energy transport*. (2002).

51. Lehner, B. & Grill, G. Global river hydrography and network routing: baseline data and new approaches to study the world's large river systems. *Hydrol. Process.* **27**, 2171–2186 (2013).

52. Danielson, J. J. & Gesch, D. B. Global multi-resolution terrain elevation data 2010 (GMTED2010). *US Geol. Surv. Open File Rep* **1073**, 25 (2011).

53. Gleeson, T., Moosdorf, N., Hartmann, J. & van Beek, L. P. H. A glimpse beneath earth's surface: GLobal HYdrogeology MaPS (GLHYMPS) of permeability and porosity. *Geophys. Res. Lett.* **41**, 1–8 (2014).

54. Gleeson, T. *et al.* Mapping permeability over the surface of the Earth. *Geophys. Res. Lett.* **38**, 1–6 (2011).

55. Döll, P. & Fiedler, K. Global-scale modeling of groundwater recharge. *Hydrol. Earth Syst. Sci.* **12**, 863–885 (2008).

56.   Gleeson, T. & Manning, A. H. Regional groundwater flow in mountainous terrain: Three-dimensional simulations of topographic and hydrogeologic controls. *Water Resour. Res.* **44**, (2008).

57.   Fan, Y. & Schaller, M. F. River basins as groundwater exporters and importers: Implications for water cycle and climate modeling. *J. Geophys. Res. Atmos.* **114**, (2009).

58.   Muis, S., Verlaan, M., Winsemius, H. C., Aerts, J. C. J. H. & Ward, P. J. A global reanalysis of storm surges and extreme sea levels. *Nat. Commun.* **7**, (2016).

59.   Fan, Y., Li, H. & Miguez-Macho, G. Global patterns of groundwater table depth. *Science (80-.).* **339**, 940–943 (2013).

60.   Younger, P. L. Submarine groundwater discharge. *Nature* **382**, 121–122 (1996).

61.   Burnett, W. C. *et al.* Quantifying submarine groundwater discharge in the coastal zone via multiple methods. *Sci. Total Environ.* **367**, 498–543 (2006).

62.   Stewart, B. T., Santos, I. R., Tait, D. R., Macklin, P. A. & Maher, D. T. Submarine groundwater discharge and associated fluxes of alkalinity and dissolved carbon into Moreton Bay (Australia) estimated via radium isotopes. *Mar. Chem.* **174**, 1–12 (2015).

63.   Cole, J. J. *et al.* Plumbing the global carbon cycle: integrating inland waters into the terrestrial carbon budget. *Ecosystems* **10**, 172–185 (2007).

64.   Beusen, A. H. W., Slomp, C. P. & Bouwman, A. F. Global land–ocean linkage: direct inputs of nitrogen to coastal waters via submarine groundwater discharge. *Environ. Res. Lett.* **8**, 034035 (2013).

65.   Potter, P., Ramankutty, N., Bennett, E. M. & Donner, S. D. Characterizing the Spatial Patterns of Global Fertilizer Application and Manure Production. *Earth Interact.* **14**, 1–22 (2010).

66.   Seitzinger, S. P. *et al.* Global river nutrient export: A scenario analysis of past and future trends. *Global Biogeochem. Cycles* **24**, (2010).

67.   Laruelle, G. G. *et al.* Anthropogenic perturbations of the silicon cycle at the global scale: Key role of the land-ocean transition. *Global Biogeochem. Cycles* **23**, (2009).

68.   Luijendijk, E. GroMPy-couple: Coupled density- driven groundwater flow and solute transport model using Python. (2019). doi:10.5281/zenodo.2616534

Supplementary information

The supplementary information is divided in six sections: S1) Geospatial data analysis of coastal watersheds, S2) Numerical model of coastal groundwater discharge, S3) Calculating global distributed coastal groundwater discharge, S4) Assessment of solute transport and eutrophication risk, S5) Sensitivity analysis and S6) Model-data comparison. The first four sections provide more details on the methods to calculate coastal groundwater discharge and the last two provide more detailed information on the model results.

S1: Geospatial data analysis of coastal watersheds

We analyzed watershed length scale, topographic gradient, groundwater recharge and near-surface permeability for n=40082 watersheds globally. The results are shown in Fig. S1 and Table S1.

Watershed geometry

We used the geometry of coastal watersheds as a first order estimate of the size of the area that contributes to coastal groundwater discharge. We acknowledge that groundwater flow does not necessarily follow surface water divides. In many cases the majority of groundwater flow is local, which means it discharges in the nearest surface water feature and surface watersheds can be a good approximation of the size of contributing areas [1]. However, in areas with high permeability, high relief or low recharge the watertable can be decoupled from topography and regional flow that bypasses the nearest discharge points can be significant[2,3]. Comparison of recharge and discharge estimates in river basins indicates that for the majority of basins the regional flow component is less than 50%[4]. To cover the uncertainty of the contributing area in our calculations of coastal groundwater discharge, we used a value of two times the size of surface watersheds as a maximum estimate.

First, 40,082 coastal watersheds were selected using global watershed [5] and coastline [6] datasets. Second, the local watershed divide to the ocean for each watershed was identified using GIS tools. The local watershed divide was defined as the boundary between each watershed and adjacent non-coastal watersheds. The representative length scale was taken as the mean distance of the water divide to the coastline. For watersheds that were only bound by other coastal watersheds we used the mean distance of the centroid of the watershed to the coastline as a representative length scale.

Note that the global analysis may underestimate coastal groundwater discharge in several tropical islands in the Pacific, since islands such as Hawaii and Mauritius are missing from the global watershed database [5] that supports the analysis.

Permeability

Permeability of each coastal watershed was extracted from a global dataset of near-surface permeability (up to ~100 m depth) [7]. The permeability map is based on a high-resolution global map of surface lithology [8] and a compilation of large-scale permeability estimates of near-surface geological units [9]. We made two changes compared to the permeability map with the aim of ensuring that the modeled coastal groundwater discharge is a high, but still conservative and realistic estimate.

In the global permeability map, areas in which the lithology consisted of mixed unconsolidated sediment or unconsolidated sediments with an unknown grain size were assigned a relatively low permeability (10^{-13} m^2) [9]. This value is below the threshold for generating significant coastal groundwater discharge, except for settings with a very high topographic gradient. However the multimodal distribution of this unit [9] suggests that in many cases this unit contains coarse grained sediments. In layered unconsolidated sediments, the effective permeability is likely to be close to the value of the most permeable sub-unit, whereas the permeability value assigned in the global permeability map is the mean permeability on a log scale. We instead assume that the permeability for coarse-grained unconsolidated sediments ($10^{-10.9}$ m^2) is more appropriate to simulate regional groundwater flow in coastal aquifers consisting of mixed or unknown unconsolidated sediments.

The permeability of carbonates in the global permeability map is likely underestimated in coastal areas with strong karstification. Coastal carbonates are predominantly karstified [10], in part because the fresh-salt water mixing zone at the coastline promotes dissolution and the formation of permeable karst conduits [11]. We therefore adopted a higher permeability estimate equal to the value reported in the global permeability map plus one standard deviation ($10^{-10.3}$ m^2). While we acknowledge that this value is highly uncertain as a global average for coastal karst aquifers, and that in reality their permeability is likely to be highly variable, this value is in line with reported values of regional-scale permeability in coastal karst aquifers [12–14].

Groundwater recharge

Groundwater recharge was derived from a calibrated global groundwater model[15]. We also used an older global recharge model[16], which generally predicts lower values of recharge and was used as a lower bound for the uncertainty analysis of global submarine groundwater discharge.

Topography

Elevation data[17] was extracted for each coastal watershed. We calculated distance to the coastline and elevation for each point in the elevation raster. We then calculated the average and standard deviation of the topographic gradient by dividing elevation by the distance to the coast. In addition, we calculated the topographic gradient for raster cells that contained a stream. The locations of streams were obtained by grouping raster cells for which the distance to the coast is the same within a range that is equal to the size of one raster cell, and then selected the raster cell with the lowest elevation for each distance value. In addition we extracted the average topographic gradient for the first 1000 m from the coastline.

Additional geospatial datasets

We extracted a number of global datasets for a comparison with the calculated submarine and terrestrial discharge, including river discharge[15], potential evapotranspiration[18], the elevation of tide and storm surges[19] and watertable gradient, which was quantified using a global model of watertable depth[20] and global elevation datasets[17].

S2: Numerical model of groundwater flow in coastal aquifers

We modeled coupled density-dependent groundwater flow and solute transport in coastal aquifers using a new model code, GroMPy-couple, which is a Python shell around the generic finite element code escript[21,22]. Escript is used to solve the governing equations for coupled solute transport and density-driven groundwater flow. The choice for escript was motivated by the fact that the code runs on parallel computing facilities which strongly increases computational efficiency and by the Python interface of escript, which provides a tool for the automated execution and analysis of large numbers of model runs. An alternative like the more well-known model code SEAWAT[23] was not used because the finite difference scheme used by SEAWAT does not allow local grid-refinement around an inclined fresh-salt water interface in coastal aquifers. While we did initially use the finite element code SUTRA[24], SUTRA at present does not offer parallel computation, has no Python interface to allow executing multiple model runs, and does not have facilities to halt transient model runs when they have reached steady-state. Escript has been used to simulate density-driven fluid flow and reactive transport in a number of studies[21,22,25,26], although this is to our knowledge the first time it has been applied to model coastal groundwater flow.

Governing equations

Density dependent groundwater flow was modeled by solving the following equation [27]:

$$S\frac{\partial P}{\partial t} + \phi\gamma\frac{\partial C}{\partial t} = \nabla\frac{\rho_f k}{\mu}(\nabla P + \rho_f g\nabla z) + Q_f \qquad \text{(S1)}$$

Where S is storativity ($s^2 m^{-2}$), P is pressure (Pa), t is time (sec), C is solute concentration ($kg\ kg^{-1}$), ρ_f is fluid density ($kg\ m^{-3}$), ϕ is porosity (dimensionless), γ is solute expansion coefficient (dimensionless), k is permeability (m^2), μ is dynamic viscosity ($Pa\ s$), g is the gravitational constant (9.81 $m\ s^{-2}$), z is elevation (m) and Q_f is a fluid source or sink ($kg\ m^{-3}\ s^{-1}$). Solute transport is given by [27]:

$$\frac{\partial(\rho_f C)}{\partial t} = \nabla\rho_f D_h\nabla C - \vec{v}\ \nabla(\rho_f C) + \frac{Q_f C_s}{\phi} \qquad \text{(S2)}$$

Where D_h is the dispersion coefficient tensor ($m^2\ s^{-1}$), $\vec{v}$ is flow velocity ($m\ s^{-1}$) and C_s is solute concentration of the fluid source or sink ($kg\ kg^{-1}$). The hydrodynamic dispersion tensor D_h is calculated as [28]:

$$D_{h,xx} = \frac{v_x^2}{|v|}\alpha_L + \frac{v_z^2}{|v|}\alpha_T + D_m \qquad \text{(S3a)}$$

$$D_{h,zz} = \frac{v_x^2}{|v|}\alpha_T + \frac{v_z^2}{|v|}\alpha_L + D_m \qquad \text{(S3b)}$$

$$D_{h,xz} = D_{h,zx} = (\alpha_L - \alpha_T\frac{v_x v_z}{|v|}) \qquad \text{(S3c)}$$

Where α_L and α_T are the longitudinal and transverse dispersivity coefficient, respectively (m), and $|v|$ is the absolute value of groundwater velocity ($m\ s^{-1}$).

Flow velocity v is calculated as:

$$v = \frac{k}{\mu\phi}(\nabla P + \rho_f g\nabla z) \qquad \text{(S4)}$$

Fluid density and viscosity are calculated using a linear equation of state and assuming a constant temperature and pressure:

$$\rho_f = \rho_w + \rho_w\gamma C \qquad \text{(S5)}$$

$$\mu = \mu_0 + aC \qquad \text{(S6)}$$

Where ρ_w and μ_0 are the density (kg m^{-3}) and viscosity (Pa s) of pure water, respectively, and γ and a are dimensionless constants. Values of ρ_w, γ, μ_0 and a are listed in Table 2 and were found using linear regression to published equations of state [29] over the range of salinities of 0.0 to 0.035 kg kg^{-1}.

Solving the flow and solute transport equations

The solute transport and groundwater flow equations were solved using the finite element code escript[21,22]. We follow an iterative coupling algorithm[30] in which the solute transport equation (equation S2), equations of state (equations S5 and S6) and groundwater flow equations (equations S1 and S4) are solved iteratively until the change in pressure and concentration between two iterations is less than 1×10^{-4} Pa and less than 1×10^{-7} $kg\ kg^{-1}$, respectively.

Model geometry

Groundwater flow was simulated in a two-dimensional cross section of the subsurface. While we acknowledge that coastal groundwater flow is a three dimensional process, the computational demands of running large numbers of three dimensional models would be prohibitive, given the high spatial resolution required to accurately model density-driven flow and the constraints on timestep size imposed by numerical stability of modeling advective solute transport[31].

We assigned a constant linear slope to the terrestrial and marine parts of the model domain. The linear slope is a simplification. Testing more complex topographies, with for instance a lower slope of the near-shore parts that is often found in sedimentary settings, or conversely high relief and cliffs in erosional settings would increase the number of model runs that are needed to cover parameter space significantly, and would make the computational costs prohibitive. We therefore aimed to cover the first order effects of a linear topography for the study presented here.

The first 1000 m of the model domain are covered by seawater. The length of the landward size of the model was constrained by the watershed length described in section S1. The thickness of the model domain was kept at 100 m for the exploration of the parameter space, and was varied between 100 and 500 m for sensitivity analysis.

We applied a spatial discretization that varied from 3 m in a zone that extends 500 m offshore and 250 m onshore to 10 m on the landward boundary of the model domain. The zone with fine discretization is centered around the fresh-salt water interface that was calculated using an analytical solution[32]:

$$y^2 = 2\frac{\rho_f Q}{(\rho_s - \rho_f)K}x + \left(\frac{\rho_f Q}{(\rho_s - \rho_f)K}\right)^2 \qquad\qquad \text{(S7)}$$

Where y is the depth of the interface below sea level (m), K is hydraulic conductivity (m s^{-1}), which is calculated as $K = \rho_f g\kappa/\mu$, ρ_f and ρ_s are the density of freshwater and seawater, respectively (kg m^{-3}), Q is the discharge rate of fresh groundwater (m^2 s^{-1}) and x is distance to the coastline (m). The discharge term (Q) in eq. S7 was calculated using a depth-integrated version of Darcy's law:

$$Q = Kb\frac{\partial h}{\partial x} \qquad\qquad \text{(S8)}$$

Where b is aquifer thickness (m), and h is hydraulic head (m). In case the calculated discharge exceeded the total recharge input (i.e., the product of the recharge and length of the model domain) into the system, discharge was capped to equal the recharge input.

Initial and boundary conditions

A specified recharge flux boundary and a seepage boundary condition were applied to the upper model boundary at the terrestrial side of the model domain. For the seaward side of the model domain we applied a specified pressure that equals the load of the overlying seawater. Initial salinity was equal to seawater values of 0.035 kg kg^{-1} under the seabed and in a saltwater toe that extends inland following equation S7. Initial pressures were calculated by solving the steady-state version of the groundwater flow equation (eq. S1).

The exchange of groundwater and surface water or evapotranspiration was simulated using a seepage boundary algorithm[33]. The seepage algorithm was chosen because it represents a more realistic upper boundary than often used fixed specified pressure or flux boundaries, while avoiding the computational cost of explicitly modeling evapotranspiration and surface-groundwater exchange. The seepage boundary condition was implemented using an iterative procedure. First, initial pressures were calculated by solving the steady-steady-state groundwater flow equation (eq. S1, with the derivative of pressure and concentration over time set to zero). For the first step a specified flux was assigned to the entire top boundary, which represents groundwater recharge from precipitation. Following the first iteration step, a specified pressure boundary was adopted at any surface node where the fluid pressure (P) exceeds 0 Pa. Fluid pressures were then recalculated again by solving eq. S1 using this new boundary condition. Following each iteration step, the flux to the boundary nodes was calculated by solving the steady-state groundwater flow equation. Any surface nodes where the fluid pressure exceeds 0 Pa are added to the seepage boundary and are assigned a specified pressure of 0 Pa. Seepage boundary nodes that instead of outflow generate inflow into the model domain at a rate that exceeds the recharge rate were removed from the seepage boundary. To avoid oscillations in the solution, only the nodes that generate 10% or more inflow compared to the seepage node with the highest rate of inflow are removed from the boundary condition after each iteration. This iterative procedure is continued until the number of seepage nodes reaches a steady value.

The iteratively calibrated steady-state seepage boundary is used as an initial seepage boundary during the transient model runs. At each timestep, the active seepage boundary is inherited from the previous time step. The seepage boundary condition is removed for any node that has become a net source of water into the model domain. Any non-seepage node at the surface where the fluid pressure exceeds 0 Pa is added to the seepage boundary. This implementation of the seepage boundary condition ensures that the hydraulic head never exceeds the surface elevation, and that there is not more inflow than the specified recharge rate at any node at the surface. Both possibilities would be unrealistic, but allowed when either a specified flux or a specified pressure boundary condition would be used for the upper boundary. In addition, the seepage boundary method as implemented here avoids the use of an unknown and uncertain drain conductance

parameter that is used in drain boundary conditions, which aim to provide a similar realistic upper boundary as the seepage boundary[33] but use a different algorithm to achieve this.

Assumption of constant thickness and saturation

The model domain was assumed to be fully saturated and the saturated thickness was constant in the model domain and independent of the modeled pressures and hydraulic head. This is a simplification that avoids the numerical instability and high computational costs of modeling unsaturated groundwater flow in combination with density-driven flow. At the same time it makes comparisons between the individual model runs easier, because saturated thickness and transmissivity remain constant unless permeability is changed. In addition, when not adopted, the modeled thickness of the model domains for the different model scenarios would have to be sufficiently high to accommodate all possible modeled hydraulic gradients, which vary from values close to the highest modeled topographic gradients to values of near zero for the different model scenarios. This would again result in a prohibitively high number of model runs that would be required to cover the range found in coastal groundwater systems.

The assumption of a fully saturated subsurface does introduce errors in the modeled flow field. For models with a high topographic gradient there is a significant vertical flow component in our model setup, regardless of the shape of the watertable and the hydraulic gradient. However, for cases where permeability is high, the hydraulic gradient would relatively low and groundwater flow would in reality be nearly horizontal. The error in the partitioning between horizontal and vertical components of the flow vectors is expected to be equal in magnitude to the difference in topographic gradient and the modeled hydraulic gradient. The median difference between topographic and watertable gradient is 0.17%, and exceeds 5% in 2381 of the 40082 modeled watersheds. This error however reduces to near zero close to the shoreline, where in all model experiments the watertable was located at or very close to the surface, and where therefore the assumption of fully saturated conditions is correct. Given the fact that the near-shore part of the model domain is by far the most critical for our model results on submarine and near-shore groundwater discharge, we expect the assumption of fully saturated conditions to not significantly influence the results reported here.

We used a constant thickness over the model domain. The thickness was varied between 50 and 500 m in a first sensitivity analysis. For the final model runs we adopted a standard thickness of 100 m, which is equal to the median aquifer thickness that were used to compile data for the global permeability map[7,9], and is roughly equal to the thickness where the majority of young groundwater and active groundwater circulates following global compilations of radiogenic isotope data of

groundwater[34,35]. Adopting a standard thickness of 100 m ensures that the modeled values of transmissivity (the product of permeability and thickness) are consistent with the global permeability map.

Model runtime

The transient models were run until a steady state was reached. We assumed that the model has reached steady state when the change in pressure is less than 1 Pa a^{-1} and the change in solute concentration that is less than 1×10^{-4} kg kg^{-1} a^{-1}. The initial timestep size was 5 days and was increased by a factor of 1.03 after completing each timestep. To avoid numerical instability in solving advective solute transport, the maximum size of the timestep was adjusted automatically to not exceed the Courant-Friedrichs-Lewy (CFL) condition[36]:

$$CFL = q \, \Delta t \, / \, \Delta x \qquad (S9)$$

where q is fluid flux (m s^{-1}), Δt is timestep size (s) and Δx is the size of one element (m) as calculated by escript [21]. We used a relatively low limiting value of CFL=1.0 to ensure numerical stability for the large set of different models that we tested.

Model validation

To assess how well the model can simulate fresh and salt water discharge in coastal aquifer systems we compared the model code with experimental data from a salt water intrusion experiment[37], with analytical solutions of terrestrial groundwater discharge[33,38] and comparison of modeled coastal discharge fluxes with the widely used model code SUTRA[24].

The published salt-water intrusion experiment[37] consists of a tank filled with porous material that is in contact with a column of salt water on one side and a column of fresh water on the other. A hydraulic gradient is imposed from the fresh water side to the salt water side, which causes a net freshwater flow across the model domain. Over time a salt water wedge forms at the salt-water edge of the tank. The position of the salt wedge and the rate of freshwater discharge are strongly affected by the coupling between density-driven flow and solute transport. The experiment is therefore a good benchmark for model codes of coupled flow and solute transport [37], and a better alternative to than the Henry problem [39], which a standard benchmark problem but is less sensitive to the density coupling [40]. The modeled and measured salt wedge position is show in Fig. S2 for three experiments where different hydraulic gradients were applied. The model results are close to the experimental results, with a mean absolute error of 0.01 m for the position of the fresh-salt water boundary. The modeled position of the fresh-salt water interface is identical to the position modeled with the widely used model code Sutra [24]. More importantly, the modeled freshwater discharge for the three

experiments of 1.41, 0.61 and 1.17 cm^3 s^{-1} is almost identical to the measured fluxes of 1.42, 0.59 and 1.19 cm^3 s^{-1}, respectively, which means that the modeled freshwater fluxes are relatively accurate.

The model simulates onshore discharge using a seepage algorithm [33]. The modeled extent of the area where seepage takes place was compared to an analytical solution of the seepage boundary [33], which uses Dupuit assumptions, i.e., the vertical component of groundwater flow is assumed to be zero. The results are shown in Fig. S3. Our results agree show good agreement with the analytical solution, but consistently show a slightly smaller size of the discharge zone. This is in agreement with numerical experiments by Bresciani et al. [41] who shows that the analytical solution overestimates the size of the seepage zone due to the limitations imposed by the Dupuit assumption.

The modeled discharge fluxes over the land surface were compared to an analytical solution of groundwater discharge by Bokuniewicz [38]. The analytical solution assumes a constant linear hydraulic gradient over the land domain instead of the more realistic recharge and seepage boundary that we used in GroMPy-couple. We adopted a specified hydraulic head boundary condition for three model runs that were compared to the analytical solution. The modeled discharge flux matches the analytical solution perfectly (Fig. S4).

Finally, modeled fresh and salt water fluxes were also compared to modeled fluxes by Sutra. A comparison of modeled terrestrial and submarine groundwater discharge simulated by GroMPy-couple and Sutra is shown in Fig. S5. For these model setups the upper boundary condition was simplified to a fixed watertable (i.e., fluid pressure is zero) at the land surface. This is because Sutra does not have the option to simulate a seepage boundary. All other conditions were equal to the model runs that were used to explore submarine groundwater discharge in this manuscript. The results show a good match between Sutra and GroMPy-couple. GroMPy-couple predicts slightly higher recirculated submarine groundwater discharge fluxes, with an average of 12% of the total submarine groundwater discharge being saline in the Sutra model experiments and 15% in GroMPy-couple. The cause for this is unknown. However, because the difference is very small compared to the other uncertainties (such as permeability) in modeling coastal groundwater discharge and both models show identical results in the salt-water intrusion benchmark discussed previously we consider GroMPy-couple sufficiently accurate to quantify coastal groundwater discharge.

Model sensitivity analysis and exploration of parameter space

First, we performed a sensitivity analysis of submarine groundwater discharge by varying watershed length, topographic gradient, groundwater recharge and permeability in a range covers the values found in the geospatial analysis (compare Fig. S1 and Table S1). In addition, we tested the effect of a realistic range of values of aquifer thickness and permeability anisotropy and longitudinal dispersivity

for which no data was available. The sensitivity analysis consisted of a total of 130 model runs. The parameters ranges are shown in Table 3. The base case model used the median watershed length and groundwater recharge from the geospatial analysis, and a higher permeability and topographic gradient than the median watershed to better show the sensitivity of submarine groundwater discharge to the various parameters.

Second, we conducted a number of model experiments (n=495) to explore the parameter space for recharge input (recharge multiplied by contributing area), topographic gradient and permeability. The ranges of these parameters are shown in Table S4. The length of the model domain was kept constant at 3 km in all these model runs to reduce the number of runs require to cover parameter space. This does not affect model results because the model sensitivity analysis shows that changes in recharge input by either changing the contributing area (watershed length) or the groundwater recharge rate have the same effect on modeled groundwater flow and discharge (see Fig. 1D and Fig. 1F). Apart from the recharge input, permeability and topographic gradient all other parameters were constant and followed the base case values listed in Table S3. A number of runs (n=144) did not converge to steady-state after a total number of 10,000 timesteps or were numerically unstable and were discarded. These consisted predominantly of models with a very low topographic gradient ($<10^{-3}$ m m^{-1}) or recharge rate (<0.01 m a^{-1}), where flow rates were so low that numerical precision affected the results.

Longitudinal dispersivity was kept constant at a value of 50 m and transverse dispersivity was assumed to be 0.1 times longitudinal dispersivity. Compilations of dispersivity data suggests that for the scales of the numerical models presented here longitudinal dispersivity varies between approximately 10 and 100 m, while transverse dispersivity is an order of magnitude lower [42]. However, some case studies in coastal aquifers have reported much lower numbers[43]. Nonetheless we have opted to use relatively high values of longitudinal and transverse dispersivity of 50 m and 5 m, respectively. The reason is that lower values would strongly increase the computational costs, since for lower values of dispersivity one would have to decrease the grid cell size and increase the number of grid cells.

Permeability anisotropy (the ratio of horizontal over vertical permeability) was kept constant at a value of 10. For fractured crystalline rocks vertical permeability may exceed horizontal permeability, whereas for layered sediment sequences anisotropy can reach a factor of 100 or more [44]. We used a constant anisotropy value of 10 to strike a balance between these two end-members. Note that a more accurate implementation of permeability anisotropy in our models would require information on the orientations of fractures and bedding in coastal aquifers, which are currently not available at a global scale.

Representative topographic gradient

The cross-sectional models use a simple linear topographic gradient. The topographic gradient is important because it sets a maximum for the hydraulic gradient in each watershed and because it governs the partitioning between terrestrial groundwater recharge, terrestrial discharge and submarine groundwater discharge. We evaluated two metrics as representative topographic gradient: the average topographic gradient of coastal watersheds and the topographic gradient of drainage features (ie., streams) only. To explore which metric provides the best model of coastal groundwater discharge we compared a series of numerical model runs which used a 2D map-view model that included the full topography of coastal watersheds with a series of simplified cross-sectional models. The map-view models were conducted using a standard finite difference model code of steady-state depth-integrated groundwater flow implemented in the programming language Python[45] and employed an identical seepage algorithm[33] as described previously for the cross-sectional models to simulate groundwater discharge. The map-view models include the full topography of each raster cell in the elevation dataset, and are therefore expected to provide a better estimate of groundwater recharge and discharge processes than the cross-sectional models. The map-view models simulate depth-integrated groundwater flow in a single layer, which is a common assumption in regional-scale groundwater models. The models used elevation data from a global digital elevation dataset [17], and recharge and permeability following the results of the geospatial analysis described in section S1. We simulated groundwater flow and discharge in 59 randomly chosen watersheds and compared the modeled terrestrial, near-shore and submarine groundwater flux in the map-view model with the fluxes simulated in the cross-sectional models. For this series of model runs both the map-view and cross-sectional models simulated single-density groundwater flow and did not include solute transport.

The results of a single model run for an example watershed are shown in Figure S6. A comparison of the recharge and discharge fluxes as a function of the distance to the coastline for the map-view and the cross-sectional models are shown in Fig. S6f. In total 36 % of the groundwater that is recharged discharges within 500 m of the coastline for the map view model. Groundwater discharge is distributed along topographic lows that coincide with surface water drainage features in the watershed. When projected to the distance from the coastline groundwater recharge and discharge are distributed unevenly (Fig S6f). In the cross-sectional models recharge is focused in a small area upstream and there is a large area where recharge equals discharge and the net flux over the top boundary is zero (Fig S6f). The cross-sectional model was rerun two times, each time with a different topographic gradient corresponding to the average gradient of the entire watershed and the average gradient of the main drainage channel in the watershed. The modeled discharge for

these two cases is 39 and 11% of the applied recharge, respectively. This shows that in this case the cross-sectional model with the average topographic gradient compares best to the modeled discharge in the map-view model.

Comparison of the modeled coastal discharge fluxes for cross-sectional and map-view models for 59 randomly chosen watersheds is shown in Fig. S7. For 44 out of the 59 watersheds the modeled coastal groundwater discharge as a percentage of the total recharge in the map-view model is covered by the three cross-sectional models or the difference is 10% or less. Overall, the average topographic gradient of the entire watershed and the gradient of the streams are both equally good predictor of coastal groundwater discharge, with a coefficient of determination (R^2) value of 0.51 and 0.50, respectively. While cross-sectional models clearly do not capture the full variation of groundwater recharge and discharge, overall they area a relatively good first order approximation of coastal groundwater discharge, provided that models using the average topographic gradient and the topographic gradient of streams only are both taken into account.

S3: Calculation of global distributed coastal groundwater discharge

For each watershed we looked up values of recharge input (groundwater recharge multiplied by the length of the watershed), permeability and topographic gradient. For each watershed fresh SGD was calculated by linear interpolation of the modeled fresh SGD values of the model runs with the closest values of recharge input, permeability and topographic gradient. A comparison of the modeled and interpolated values of fresh SGD is show in Fig. S8. For n=13025 watersheds the parameter values were located outside the bounds of the parameter combinations tested by the model runs. These were predominantly watersheds with in which permeability was lower than the lowest modeled permeability value (< 10^{-16} m^2). In these cases we used a nearest neighbor algorithm [46] to assign the fresh SGD value of the closest model run to the watershed. The average difference between linear interpolated and the nearest modeled fresh SGD value in log units was 0.26. We repeated the same interpolation procedure to calculate near-shore terrestrial discharge (Fig. S9), maximum discharge flux and the horizontal and vertical extent of the submarine and terrestrial discharge zone for each coastal watershed.

S4: Assessment of solute transport and eutrophication risk

First-order estimates of the solute flux that is transported by groundwater towards the oceans were calculated by multiplying the calculated global fresh SGD flux with published values for the average

concentrations of nitrogen[47,48], carbon[49], silica[50] and strontium[51] in groundwater. These estimates are based on published compilations of data predominantly from the US, which we consider as first order estimates for concentrations in groundwater at a global scale that are relatively uncertain. The estimate of carbon was based on the global average DIC in soil water of 15 mg L^{-1} as calculated from reported global DIC fluxes to the groundwater table and groundwater recharge by Kessler and Harvey [49]. The average strontium concentration in groundwater of 2.9 μM reported by Beck et al. [51] is based on compilations of groundwater strontium data and an extrapolation based on a global lithology map. The nitrogen concentration of 2 mg L^{-1} was based on a reported median value for a large dataset from the US [52]. The silica concentration was equal to a value reported by Frings et al. [53] based on a compilation of groundwater data that is predominantly from the USA. The calculated values of the global solute flux by SGD were compared to published values of the solute flux by surface runoff and earlier estimates of the contribution of fresh SGD[50,51,54,55]. Note that our estimates assume conservative transport and do not take into account fluid-rock interaction and microbial activity in coastal aquifers.

We quantify the risk of eutrophication of coastal ecosystems by the discharge of fresh groundwater and the associated nutrient load by quantifying coastal watersheds where the coastal groundwater discharge exceeds 100 m^2 a^{-1} and where nitrogen application in the adjacent coastal watershed[56] exceeds 10 kg ha^{-1}. The threshold value for coastal groundwater discharge is based on a review of locations with reported impacts of coastal groundwater discharge on ecosystems (see supplementary Table 7). The threshold for nitrogen application is an approximate lower limit for nitrogen application in areas in Europe and the USA where nitrogen concentration in the vadose zone and groundwater have increased strongly over the last century[52]. Given the very high sensitivity of coastal ecosystems and especially coral reefs to nitrogen[57], this threshold value is likely to result in a relatively conservative estimate of eutrophication risk. The calculated locations of sites with high eutrophication risk was compared with the location of sensitive ecosystems such as estuaries[58], salt marshes[59] and coral reefs[60]. We acknowledge that eutrophication of marine ecosystems is a complex function of nutrient input, transport, denitrification and mixing with seawater. The eutrophication risk reported here should be considered as a first order estimate that can guide follow up studies.

S5: Model sensitivity

The model runs that were used to calculate the global coastal groundwater fluxes use fixed values of aquifer thickness, permeability anisotropy and dispersivity. The degree to which this may affect model result is shown by results of sensitivity analysis in Fig. S10. Compared to the much more sensitive parameters topographic gradient and permeability, coastal discharge is relatively insensitive

to dispersivity and permeability anisotropy. In contrast, aquifer thickness does affect the discharge fluxes significantly. The adoption of a constant thickness for the global model results may therefore introduce significant uncertainties to the global model. We estimate this uncertainty as roughly a factor two, based on global estimates of the depth of young groundwater and active groundwater flow [34,35]. Note that this source of uncertainty is still much lower than the order of magnitude uncertainty in the global permeability dataset that was used in our analysis.

S6: Model-data comparison

Watertable gradients

We compared the modeled groundwater table gradient with a global map of watertable gradients that is based on a global compilation and model of watertable depths[20]. Note that the modeled watertable gradients were calculated by dividing the hydraulic head at the right-hand side of the model domain by the size of each model. In total 336 coastal watersheds had one or more observation of watertable depth in the global database. The comparison of the modeled and observed watertable in these watersheds shows a reasonable agreement (Fig. S11). The median ratio is 1.06, which means that our model may slightly overestimate watertable gradients and underestimate permeability and coastal groundwater discharge. The model explains slightly less than half the observed variance in watertable gradients. The coefficient of determination (R^2) is 0.57, which suggest that while overall the model matches the gradients well it does not fully capture local variability and should be considered as a first order estimate that is representative for relatively large spatial scales (i.e., watershed size, ~11 km). While a calibration of the coastal groundwater discharge model to match local watertable data would be beyond the scope of this study, the agreement between the mean modeled and observed watertables indicates that the model results presented here are relatively robust.

Comparison with local estimates of fresh SGD

The modeled values of coastal groundwater discharge and fresh SGD were compared to local fresh SGD estimates. While there are abundant estimates of total SGD in the literature studies that provide a robust quantitative estimate of the contributions of the fresh component of SGD are relatively scarce. We compiled fresh SGD estimates that were predominantly obtained using seepage meters, where the fresh component of SGD was estimated using a salinity balance of the water discharging in seepage meters[61–65] or direct sampling of discharge[66]. In addition, a number of estimates were based

on a combination of seepage meters and radon or radium isotopes in seawater[67,68], seawater salinity anomalies to estimate the fresh water contribution[69], and pore water chemistry and models of solute flux in the seabed[70]. We did not include the relatively numerous estimates of fresh SGD that were calculated using Darcy's law, because these implicitly assume that all water flowing in coastal aquifers discharges directly in the ocean, do not take into account the interaction of fresh and salt water at the coastline and diverge strongly from analytical models[38,71] or numerical models of coastal groundwater discharge like the model presented here.

Comparison of modeled and reported coastal groundwater discharge values in Fig. S12a and Table S5 shows that the modeled discharge is in several cases much lower than the values reported in many locations. Note that the reported values of fresh SGD were compared to modeled coastal groundwater discharge and not modeled fresh SGD, because in contrast to our approach the reported fresh SGD values in the literature often include water discharging above the mean sea level and below the high tide line or lack information to discern the onshore and offshore components of coastal discharge. Five studies[61,65,66,68,70] report values that are in the uncertainty range presented by our model results. The remaining five studies[62–64,67,69] show values that are one or more orders of magnitude higher than the model predictions. However, comparison of modeled values of permeability and reported values by five of these studies (see Table S5) show that with the exception of one study these values are in the same order of magnitude, and the misfit with reported fresh SGD values is not likely to be due to a systematic underestimation of permeability in our models.

Reported values of fresh submarine groundwater discharge are often equal or higher than the total recharge input in the system (Fig. S12b). All the fresh SGD estimates are from locations that have mapped rivers in the hinterland, which normally channel substantial part of the overall recharge in coastal aquifer as river baseflow and which means that only a small part of recharged groundwater can contribute to submarine groundwater discharge. Note that the reported fresh SGD values are from humid settings where models of groundwater recharge[15,16] are relatively reliable[72,73]. The contradiction between reported submarine groundwater discharge rates and the amount of groundwater available in coastal watersheds to supply fresh SGD has been noted by several previous authors[74,75]. The reasons for the mismatch may be the difficulty and high uncertainty of separating the fresh and recirculated components of SGD in local studies[76,77], and potential bias of sampling locations towards sites of relatively high and focused discharge that is visible at the shoreline[78]. Furthermore, to our knowledge sites with low or no SGD tend to not get reported in the literature.

Comparison with a karstic carbonate aquifer with no surface runoff
Initial estimates of coastal discharge assigned a permeability of $10^{-11.8}$ m^2 to carbonate units following the global permeability map. The resulting estimates of coastal discharge were lower than expected

for coastal karstic aquifers. For instance in the Yucatan peninsula surface water features are absent, and the majority of groundwater recharged is expected to discharge near the coast, along karst conduits and coastal and submarine springs[79]. Initial model runs predicted a coastal discharge of only 20% of the groundwater recharge for the eastern part of Yucatan. The modified permeability values where a higher permeability was assigned to carbonate units resulted in near-shore discharge that was equal to 87% of the groundwater recharged in the coastal watershed. This value is in accordance with discharge estimates for this region[79]. However, the total flux may still be underestimated, comparison with stream locations on Google Earth suggests that while overall the watershed and stream database[5] that support our analysis is robust, in areas with extensive karst such as Yucatan the stream density may be overestimated, which means that the representative length scale and the total groundwater input may be underestimated in our models. However, areas with continuous karstic carbonate cover over scales that exceed the scales of coastal watersheds (~11 km) are rare globally[8].

Qualitative comparison with locations of significant SGD use and reported ecosystems impacts by SGD

A comparison of modeled fresh SGD and coastal groundwater discharge with nine locations where significant use of fresh submarine groundwater has been reported[80] is shown in Table S6. In addition, a selection of seven locations that have reported strong impacts of fresh SGD on coastal ecosystems is shown in Table S7. The latter is admittedly a small sample of the large body of literature on the impacts of fresh SGD, a more extensive compilation is planned as a follow up study. In most locations that report use of fresh SGD the modeled fresh SGD exceeds 50 m^2 a^{-1} (Table S6), which is much higher than the global median discharge of 0.4 m^2 a^{-1}. In two locations (Bahrain and Quissico, Mozambique) the modeled fresh SGD is very low. However, in both cases the modeled total coastal groundwater discharge is much higher (50 and 233 m^2a^{-1}, respectively) than the fresh SGD component. Since the partitioning between fresh SGD and near-shore terrestrial discharge is highly dependent on topographic gradient the underestimation is likely due to the models not representing coastal topography well enough by using a single linear topographic gradient. The coastal (onshore and offshore) groundwater discharge in locations where effects on ecosystems have been reported (Table S7) is in most cases much higher than the median value of 30 m^2a^{-1}. The nitrogen application in the adjacent coastal watersheds are highly variable and in some cases relatively low. This suggests that either other sources of nutrients or pollutants affect the coastal ecosystems or that agricultural nitrogen application has been underestimated in the relatively low-resolution global dataset that was used[56]. In addition, in these local studies it may have been in some cases difficult to separate the effects of surface water and groundwater input. Nonetheless overall the model results successfully

match the relatively high discharges required to explain locations with significant use of fresh SGD or where coastal groundwater discharge impact the solute and nutrient budgets of coastal ecosystems.
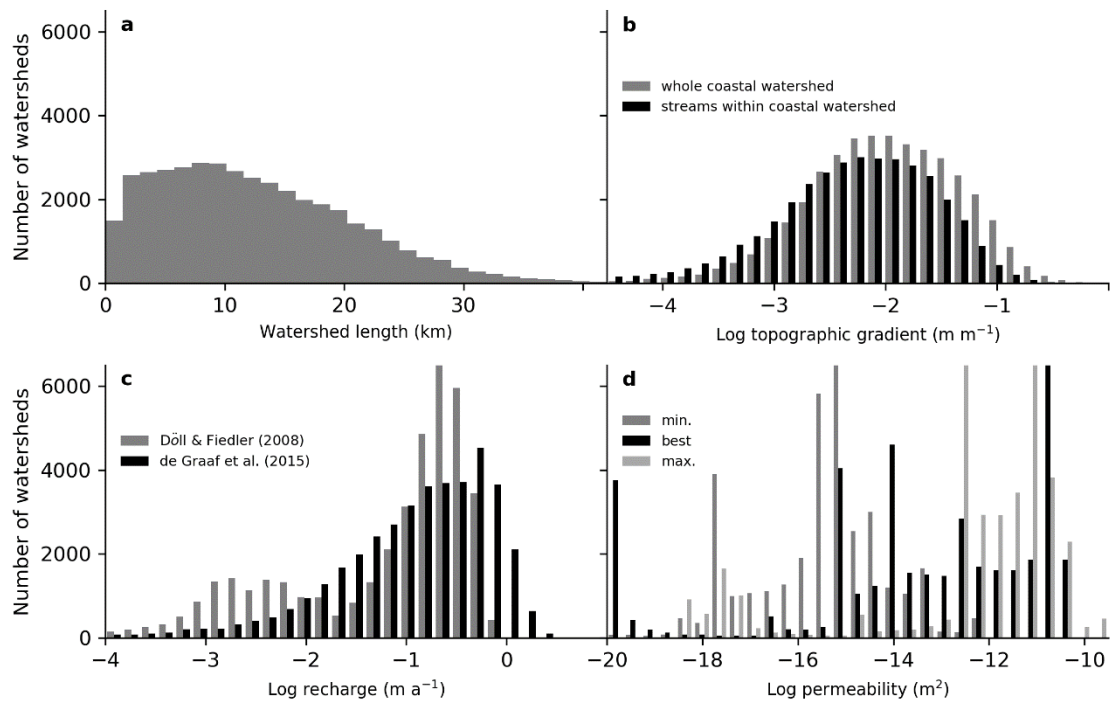
Fig. S1. Results of the global geospatial data analysis of coastal watersheds, showing representative watershed length (a), topographic gradient of coastal watersheds and streams in these watersheds (b), groundwater recharge (c) and permeability (d). The min. and max. estimates of permeability take into account the 1σ uncertainty range reported by Gleeson et al. [7,9].
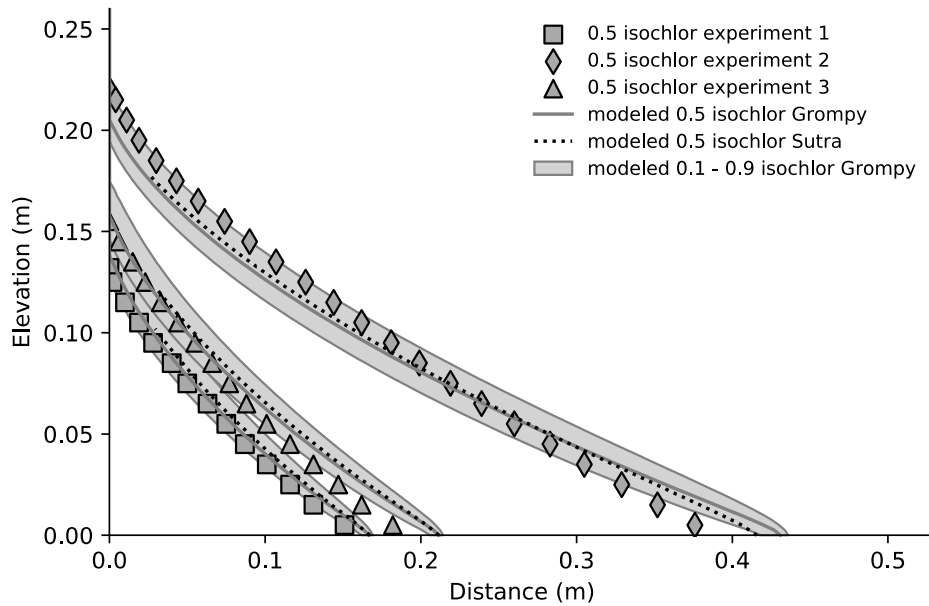
Fig. S2. Comparison of modeled position of a salt wedge by GroMPy-couple to the measured position in fresh and salt water flow experiments in porous media[37]. The modeled position of the fresh-salt water interface compares well to the measured values and is comparable to results for the widely used model code SUTRA[24]. The position of the salt wedge is equal to the location of the 50% salt water concentration contour line (0.5 isochlor).
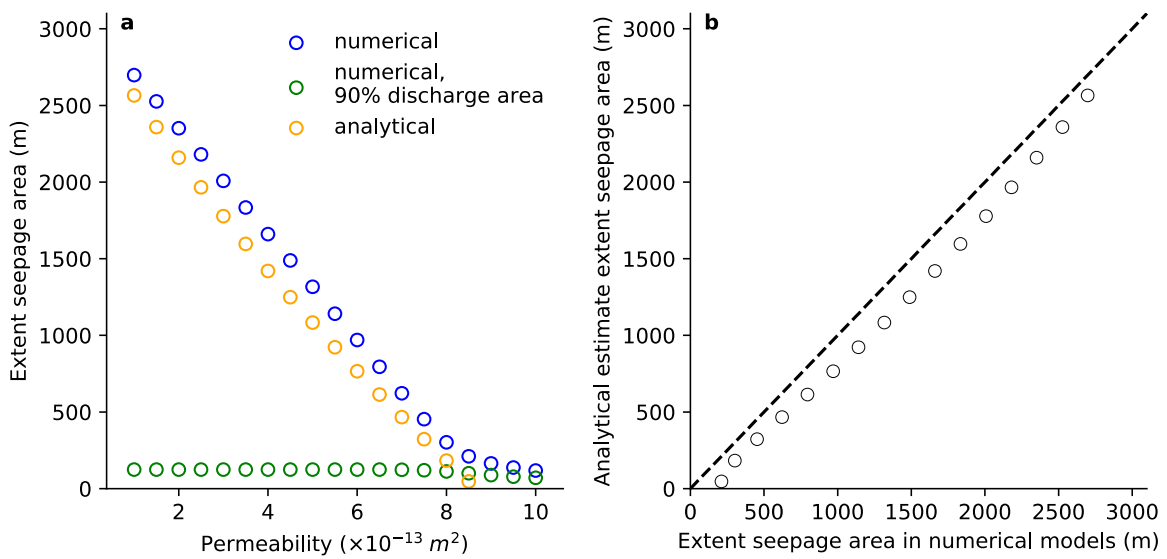

Fig. S3: Comparison of numerical estimates of the size of the onshore discharge zone with an analytical solution [33]. (a) comparison of the size of the discharge zone and permeability in a series of 20 model runs, (b) scatter plot of size of the seepage zone in numerical models and the analytical

solution. The results show good agreement between the models and the analytical solution, and confirm the moderate underestimation of seepage zones by the analytical solution reported by Bresciani et al.[41] While the seepage zone is relatively large in most model experiments, the majority of onshore discharge is concentrated near the shoreline as shown by the much smaller area where 90% of the onshore discharge takes place in panel (a). The model runs shown here used a domain length of 3000 m, a thickness of 100 m, a recharge flux of 0.1 m a^{-1} and a topographic gradient of 0.01.
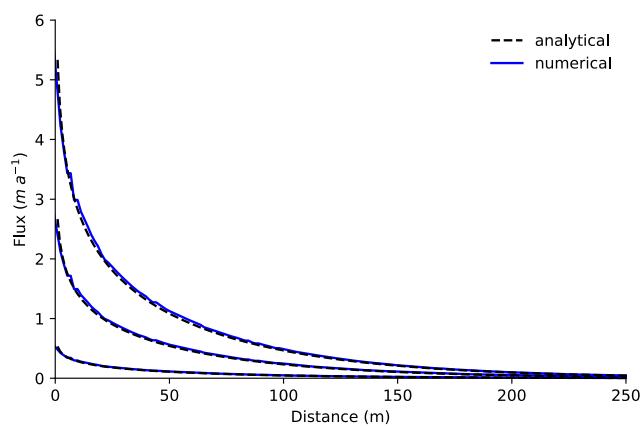

Fig. S4: Comparison of modeled groundwater discharge and calculated discharge using an analytical solution [38]. The model experiments shown used a specified pressure of 0 Pa at the entire land surface, a topographic gradient of 0.01, aquifer thickness of 100.0 m and a isotropic permeability of 10^{-13} m^2, 5.0 ×10^{-12} m^2 and 1×10^{-12} m^2.
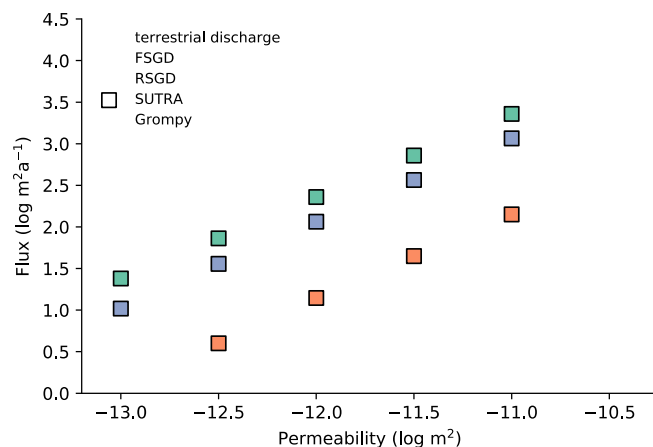

Fig. S5. Comparison of modeled fresh and recirculated submarine groundwater discharge and terrestrial discharge in a series of identical model experiments with the model codes GroMPy-couple and SUTRA. The model experiments used model domain size of 2.5 km onshore and 500 m offshore,

a topographic gradient of 0.01 and a thickness of 100 m. In contrast to the remaining model runs in this study the upper boundary did not consist of a mixed seepage and recharge boundary, but used a specified pressure of 0 Pa at the land surface.
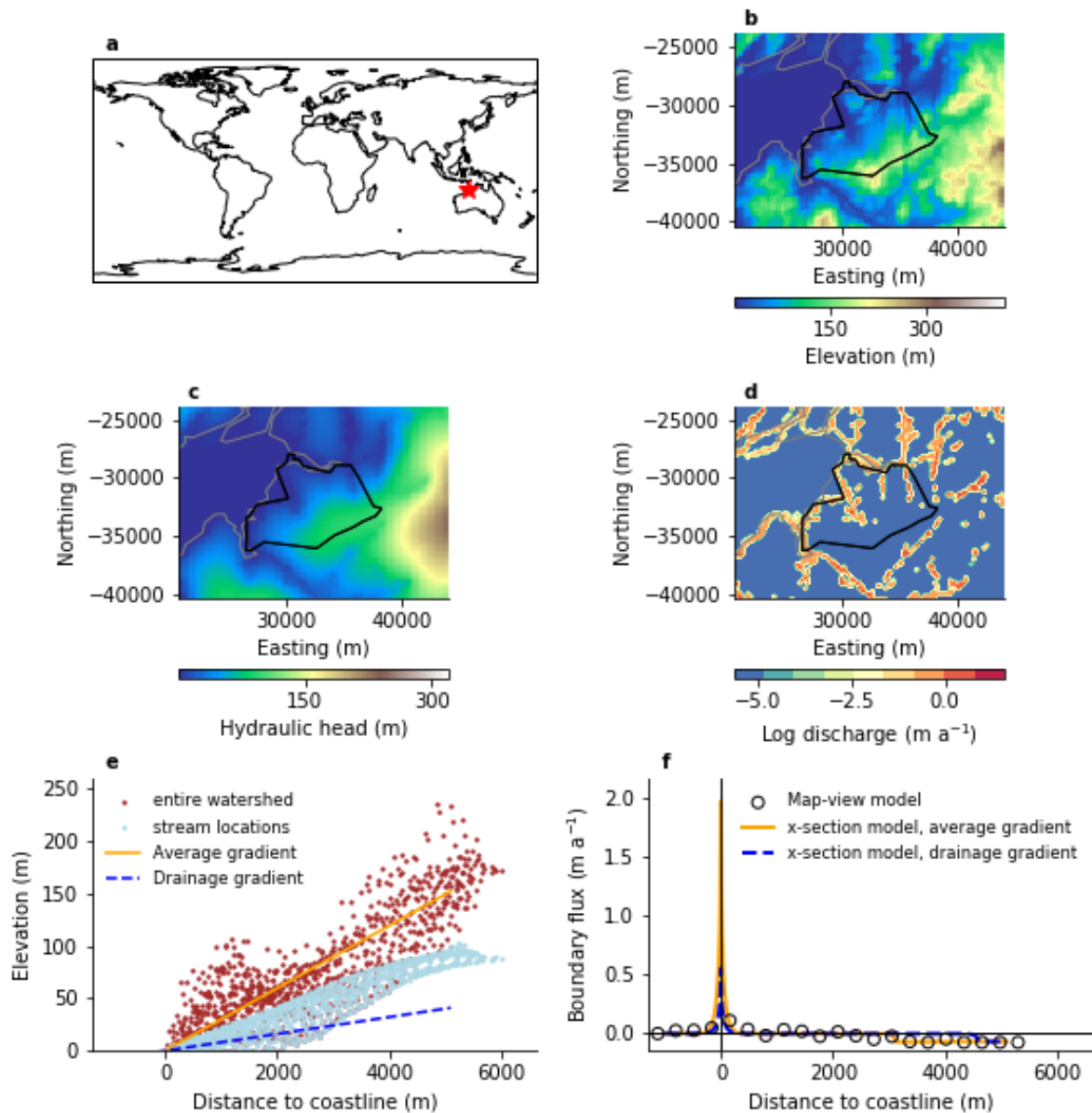

Fig. S6. Comparison of coastal groundwater flow and discharge in map-view and cross-sectional models for an example coastal aquifer in Australia. Panel b, c and d show elevation, modeled hydraulic head and modeled groundwater discharge in the map-view model. Panel e shows the elevation of the entire coastal watershed and the streams in the watershed along with two regression lines for elevation vs distance to the coast. Panel f shows the modeled groundwater discharge in the map-view model and cross-section models that use the average topography or the average topographic gradient of the streams. Overall the map-view model predicts a coastal discharge of 36% of the total recharge, and the cross-sectional model predict 39% when using the

average topographic gradient and 11% when using the gradient of the stream in the coastal watershed.
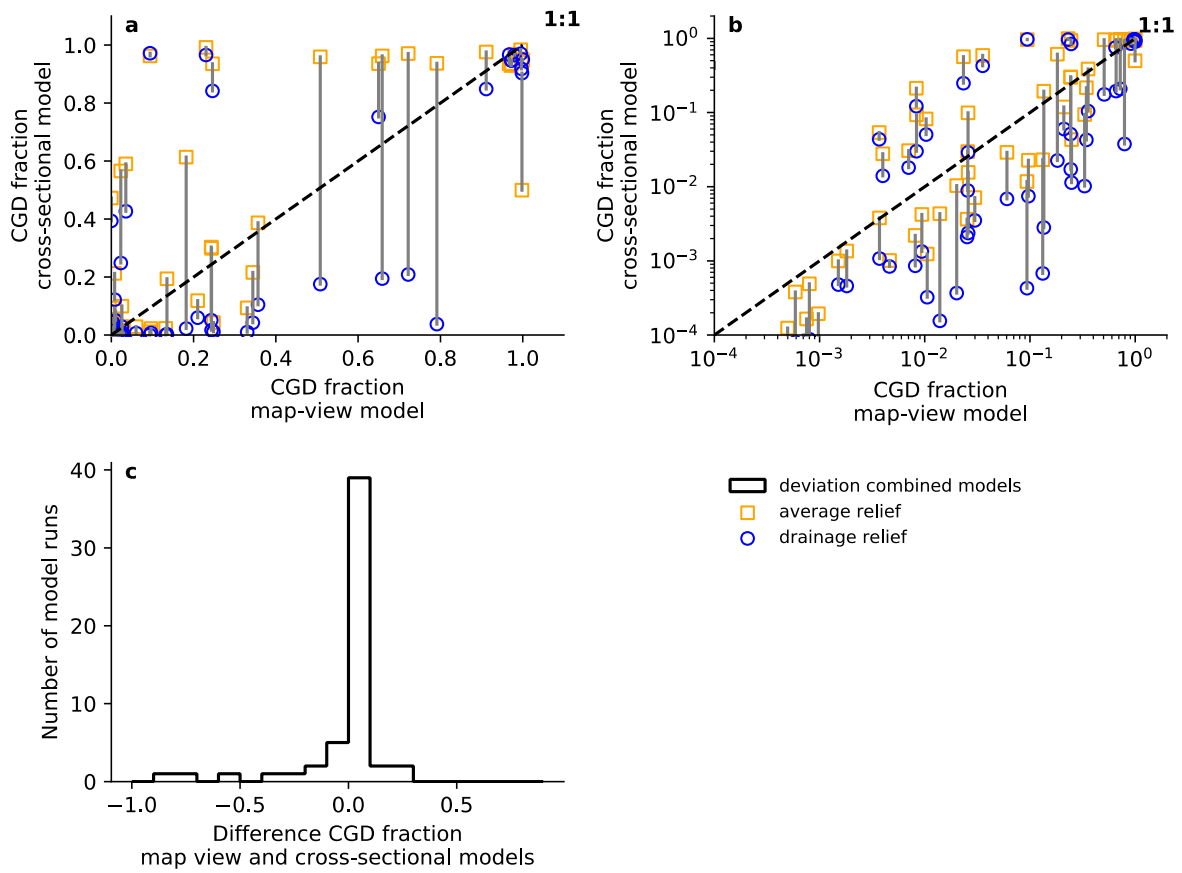

Fig. S7. Comparison of coastal groundwater flow and discharge in map-view models and cross-sectional model for 59 randomly chosen coastal watersheds. The majority of watersheds groundwater discharge can be approximated well in the 2D cross-sectional models by using either the average topographic gradient or the average gradient of the stream nodes in each watershed. For 75% of the watersheds the cross-sectional discharge falls between these values or the difference between the modeled discharge is less than 10%.
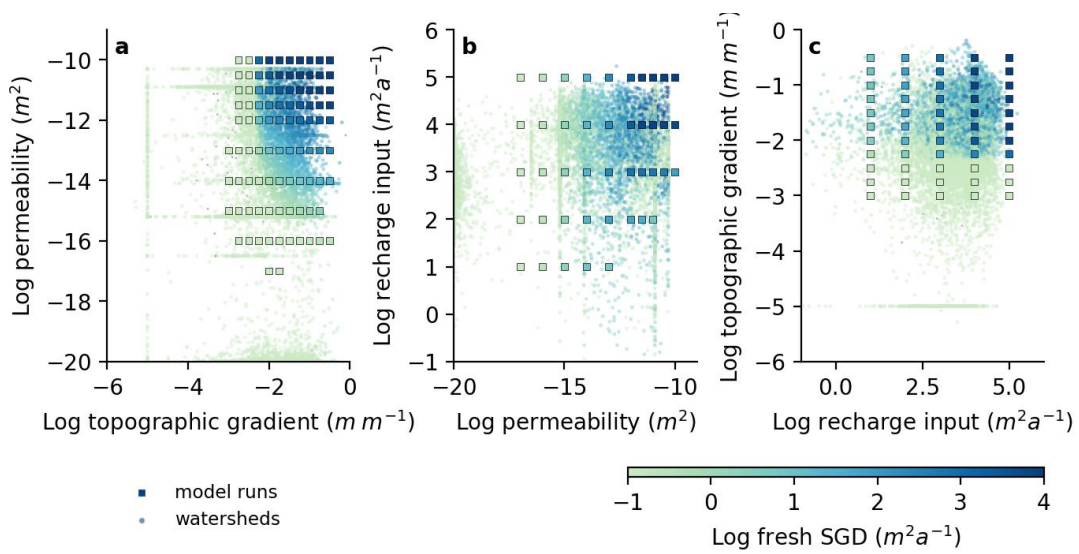
Fig. S8. Interpolation of fresh submarine groundwater discharge for each of the n=40082 coastal watersheds in our global database from n=351 model runs. Note that in each panel the model runs are shown with the highest modeled fresh SGD. For instance, for panel a behind each square there are a number of model runs that are not shown with different recharge input values.
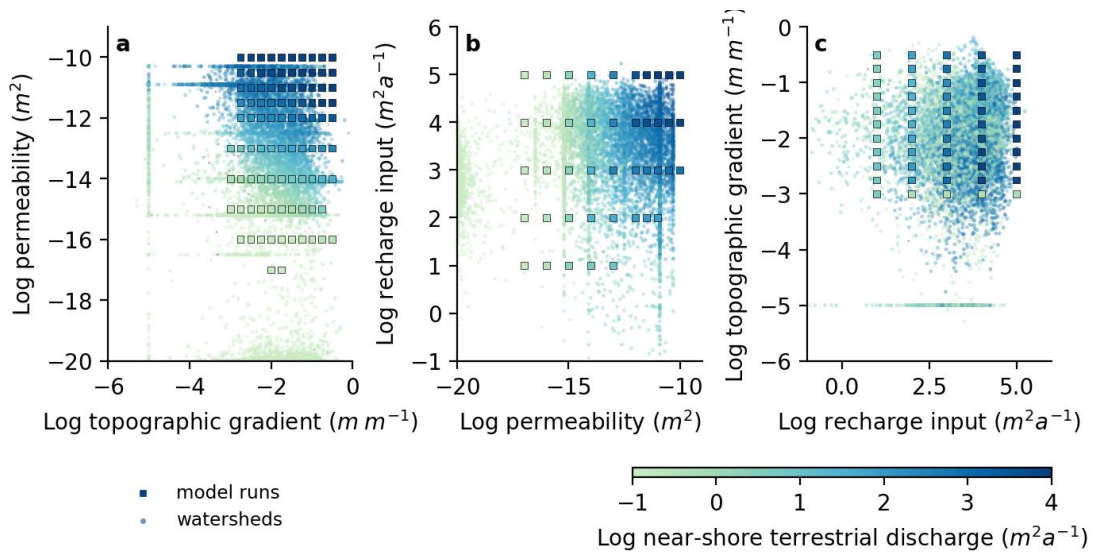
Fig. S9. Interpolation of near-shore terrestrial groundwater discharge (NGD) for each of the n=40082 coastal watersheds in our global database from n=351 model runs.
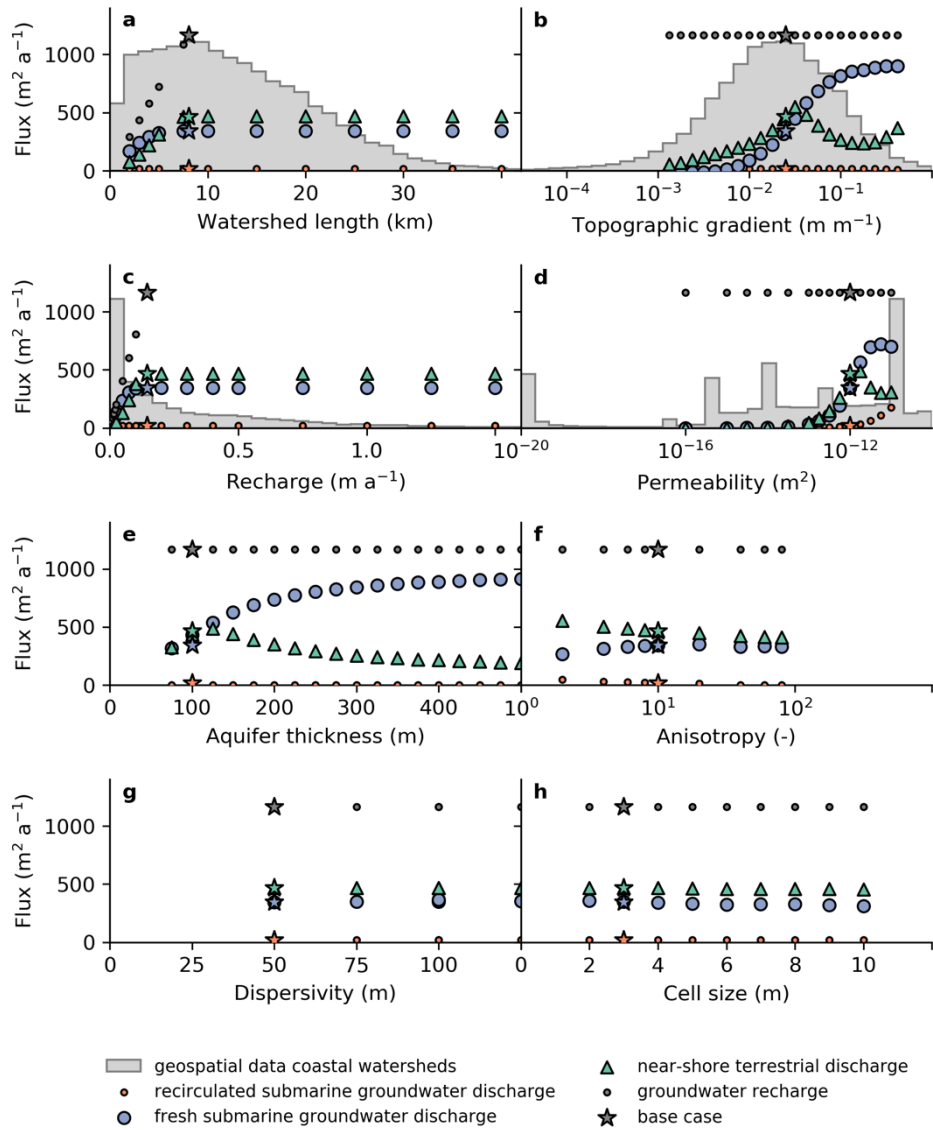
Fig. S10. Sensitivity of fresh SGD and near-shore terrestrial discharge to watershed length (a) topographic gradient (b), groundwater recharge (c), permeability (d), aquifer thickness (e), permeability anisotropy (f), longitudinal dispersivity (g) and grid cell size (h).
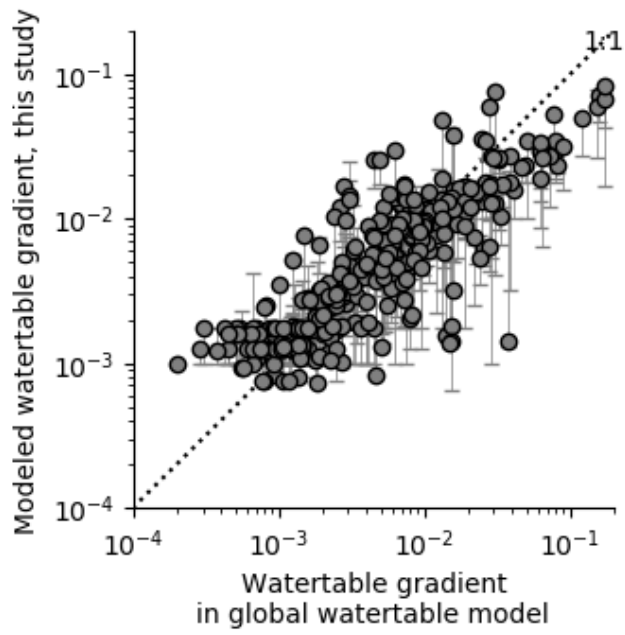
Fig. S11. Comparison of watertable gradient from a global data compilation and model[20] with the modeled watertable gradient of this study for 336 coastal watersheds with at least one watertable datapoint.
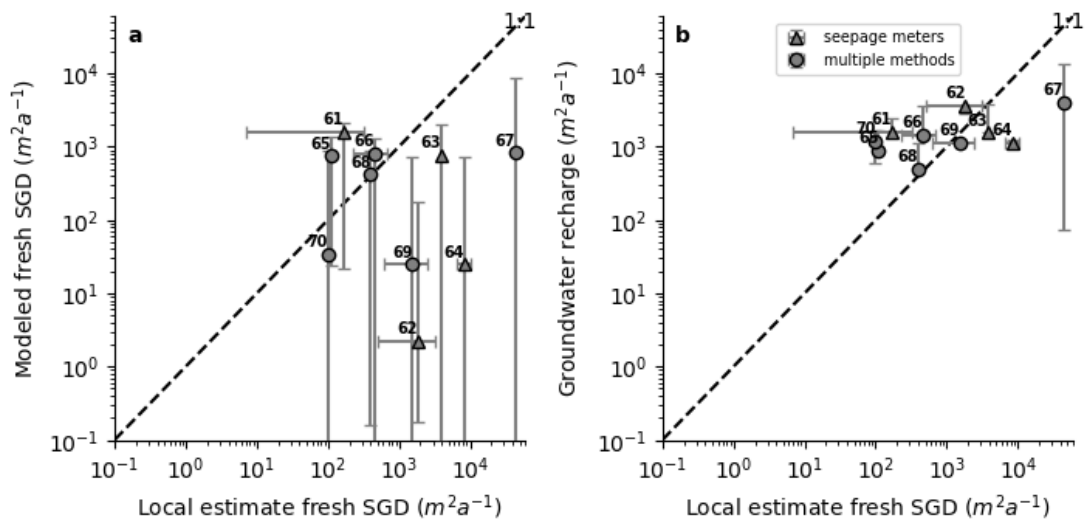
Fig. S12. Comparison of reported fresh SGD and modeled coastal groundwater discharge (A) and groundwater recharge (b). Five out of ten reported fresh SGD estimates are much higher than our model results (a), but these estimates are also equal to or exceed the total freshwater input in adjacent coastal aquifers (b). Numbers denote the reference for each estimate.
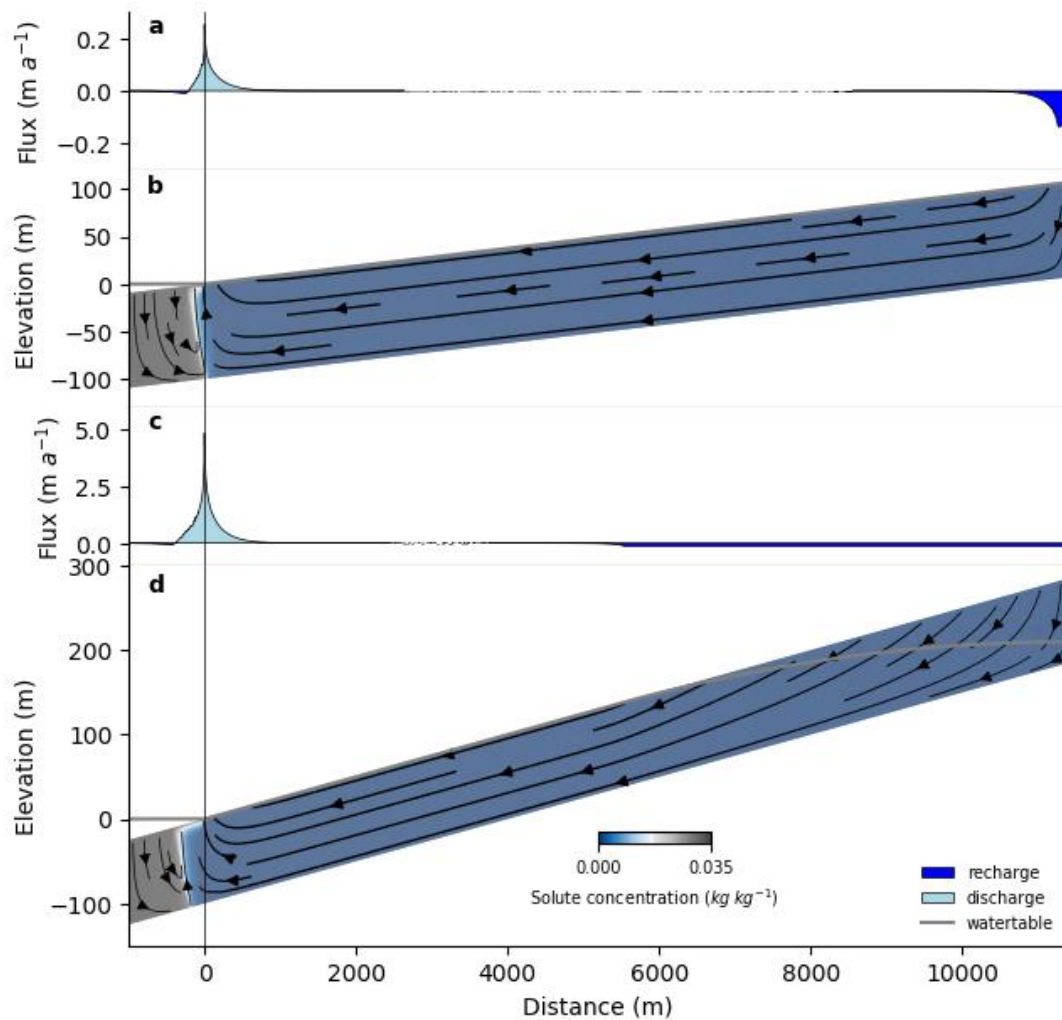
Fig. S13. Examples of modeled groundwater flow, salinity and distribution of terrestrial and submarine recharge and discharge for the median global watershed (panels a and b) and a model with a relatively high permeability (10^{-12} m^2) and topographic gradient (2.5%) (c and d). The flux over the top surface (i.e., the land surface and the seabed) is shown in panel a and c, and shows the distribution of areas with groundwater recharge (dark blue), areas with zero or near-zero discharge where the applied recharge is balanced by discharge and a relatively small zone with significant terrestrial and marine groundwater discharge (light blue).
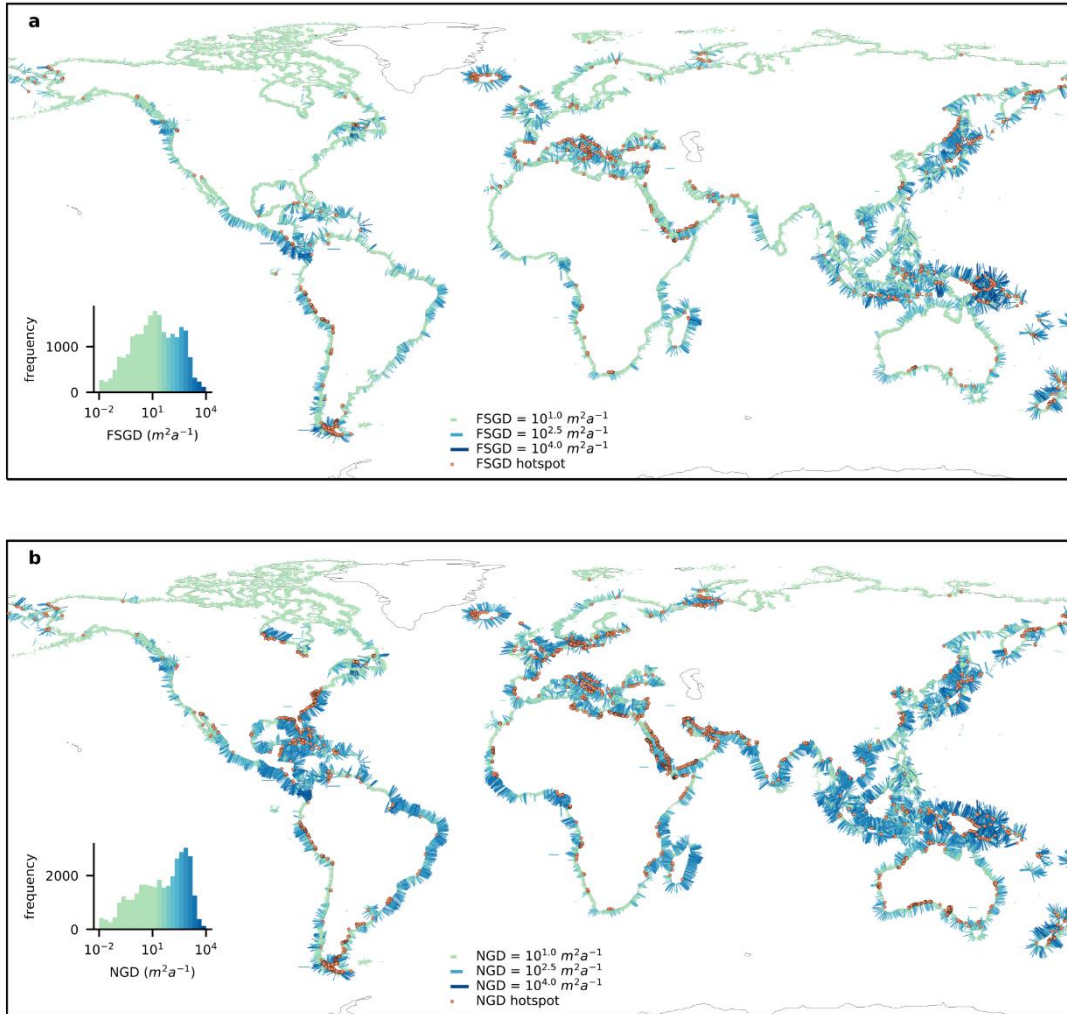
Fig. S14. Modeled fresh submarine groundwater discharge (a) and near-shore terrestrial groundwater discharge (b). Hotspots denote locations where the discharge flux exceeds 100 m²a⁻¹ and 25% of the surface water flux to the oceans.
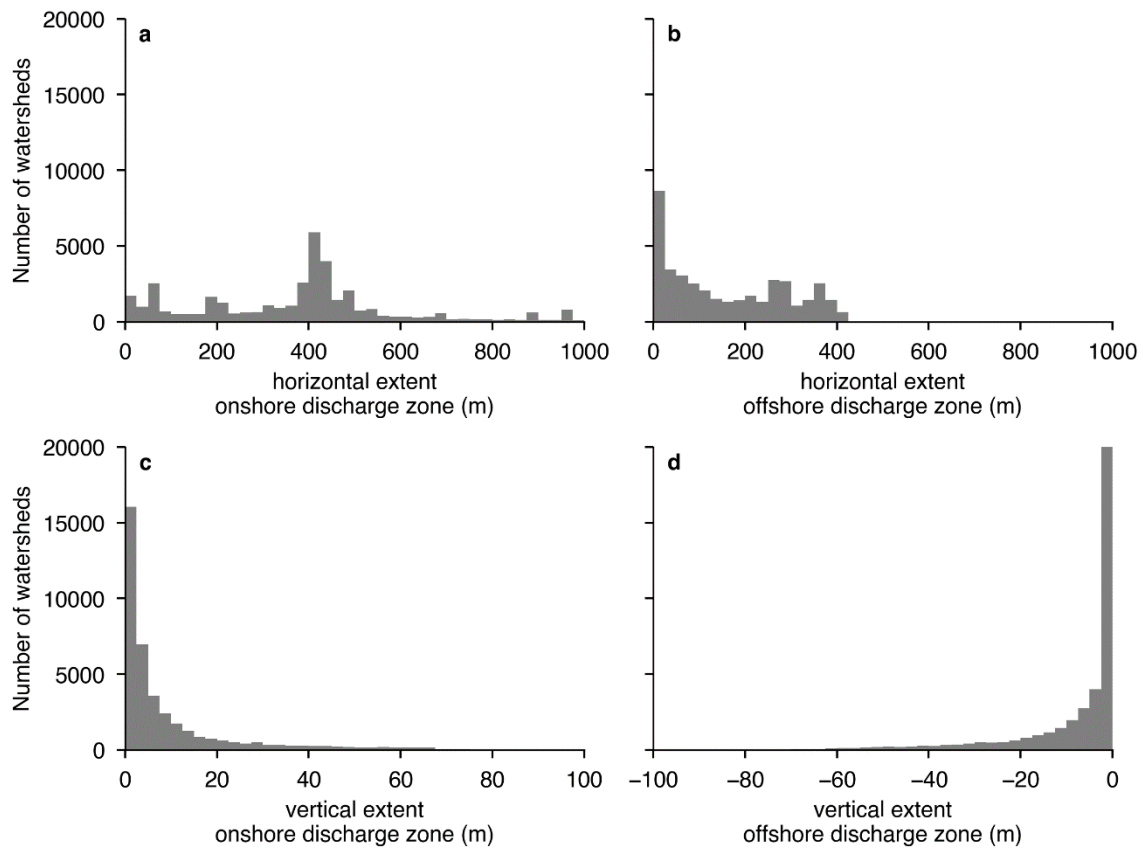
Fig. S15. Distribution of the extent (a, b) and elevation (c, d) of the modeled onshore (a, c) and offshore (b, d) coastal groundwater discharge for each global watershed. Note that these values are relatively uncertain due to the strong effect of permeability anisotropy and aquifer thickness on the location of the discharge zone, which are poorly constrained parameters in our analysis. The size of the discharge zone is defined as the area where 90% of all groundwater discharge takes place. Note that this does not include areas where discharge is equal or lower than the applied rate of groundwater recharge.
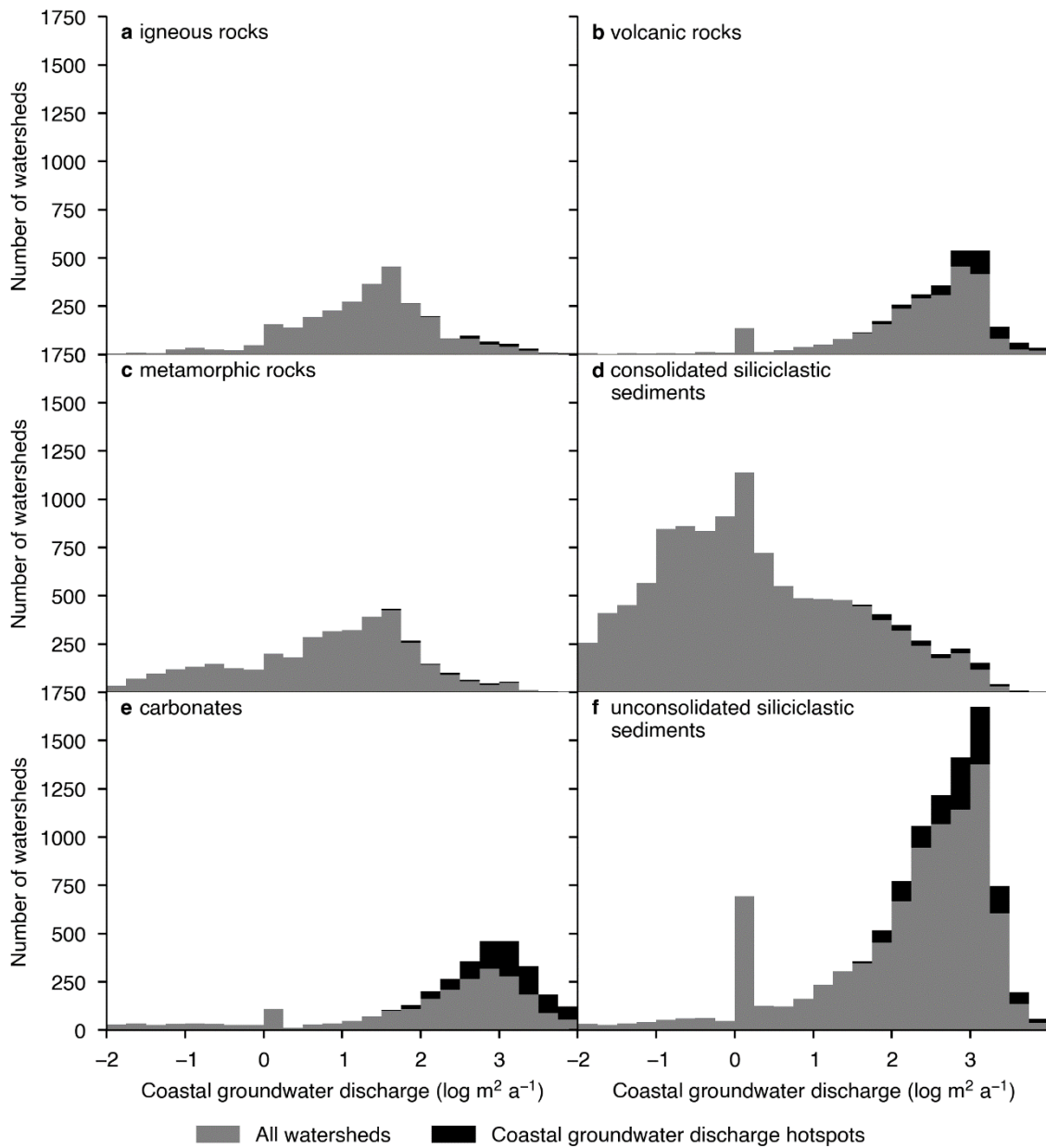
Fig. S14. The distribution of modeled coastal groundwater discharge and coastal groundwater discharge hotspots for different lithologies based on the global lithology map[8]. Model results predict that coastal groundwater discharge predominantly takes place in coastal watersheds consisting of permeable volcanic (b), carbonate (c) or unconsolidated siliciclastic rocks (f).

Table S1. Statistics for hydrogeological variables in the 40,082 global coastal watersheds.

| Variable	Units	Median	Average	Standard deviation
Watershed size	*km*	11.4	12.6	8.2
Topographic gradient, all raster cells	*m m^{-1}*	0.0094	0.025	0.043
Topographic gradient, streams	*m m^{-1}*	0.0050	0.013	0.024
Recharge [16]	*m a^{-1}*	0.132	0.167	0.164
Recharge [15]	*m a^{-1}*	0.143	0.289	0.360
Log-transformed permeability, minimum estimate	*m^2*	-15.4	-16.1	2.4
Log-transformed permeability, best estimate	*m^2*	-12.9	-13.5	2.7
Log-transformed permeability, maximum estimate	*m^2*	-11.7	-12.3	2.1

Table S2. Fixed model parameters

Parameter	Units	Value
S	*Pa^{-1}*	1.0×10^{-4}
β_w	*Pa^{-1}*	4.6×10^{-10}
ρ_w	*kg m^{-3}*	998.872
γ	dimensionless	0.6841
μ_0	*Pa s*	9.808×10^{-4}
a	*dimensionless*	2.6515×10^{-3}

Table S3. Parameters ranges used for model sensitivity analysis.

Parameter	Base case value	Sensitivity analysis values
Watershed length (m)	11400	1000, 2000, 3000, 4000, 5000, 7500, 10000, 15000, 20000, 25000, 30000, 35000, 40000
Groundwater recharge (m a^{-1})	0.143	0.001, 0.0025, 0.005, 0.01, 0.015, 0.02, 0.025, 0.05, 0.075, 0.1, 0.2, 0.3, 0.4, 0.5, 0.75, 1.0, 1.25, 1.5, 1.75
Permeability, k (log m^2)	-12	-20, -18, -17, -16, -15, -14.5, -14, -13.5, -13, -12.75, -12.5, -12.25, -12, -11.75, -11.5, -11.25, -11, -10.75, -10.5, -10.25, -10.0
Topographic gradient (log m m^{-1})	-1.6	-4 to -0.5, interval = 0.125
Aquifer thickness (m)	100	25-500, interval=25
Permeability anisotropy, (dimensionless)	10	1, 2, 4, 6, 8, 10, 20, 40, 60, 80, 100, 200
Longitudinal dispersivity, α_L (m)	50	25 to 150, interval = 25
Grid cell size (m)	3	1 to 10, interval = 1

Table S4. Parameters ranges used for the exploration of parameter space and quantifying global coastal groundwater discharge.

Parameter	Values
Recharge input (log m^2 a^{-1})	1.0 to 5.0, interval=1.0
Permeability (log m^2)	-16, -14, -13, -12, -11.5, -11, -10.5, -10
Topographic gradient (log m m^{-1})	-3 to -0.5, interval=0.25

Table S5. Comparison of modeled coastal groundwater discharge and published local estimates.

Reference	Country	Location	Reported fresh SGD (m² a⁻¹)			Method	Modeled CGD (m² a⁻¹)			Reported permeability (log m²)	Modeled permeability (log m²)
			best	min.	max.		best	min.	max.		
42	U.S.A	Stinson Beach, California	1552	631	2472	Salinity budget seawater	45	0.02	580	-10.3	-14.0
39	U.S.A.	Delaware	458	231	684	Direct sampling of discharge at low tide	664	0.04	1123	n/a	-10.9
38	Portugal	Ria Formosa	110			Seepage meters	546	26	989	n/a	-11.1
34	U.S.A	Florida river lagoon	168	7	329	Seepage meters	1026	18	1351	-11.7	-10.3
35	U.S.A.	Waquit bay	1830	505	3156	Seepage meters	3	0.05	109	n/a	-14.1
39	Brazil	Paros Lagoon	44057			Radium and salinity budget	732	0.04	10164	n/a	-11.2
36	U.S.A	Indian River Bay, Delaware	511			Seepage meters	754	0.05	1328	-11.1	-10.9
40	U.S.A	northeastern Gulf of Mexico	402			Radon and seepage meters	226	0.16	470	-11.7	-10.9
42	U.S.A	San Francisco Bay, California	100			Seepage meter and porewater chemistry model	41	0.03	642	n/a	-13.6
37	China	Yellow River Delta	8401	6575	10227	Seepage meters	45	0.02	580	-13.6	-14.0

Table S6. Modeled coastal groundwater discharge for locations with reported use of coastal groundwater [80].

Country	Location	Reported use of SGD	Modeled fresh SGD (m² a⁻¹)		
			best	min.	max.
Syria	Latakia	Collected by boat from springs 4km offshore	106	0.004	281
Lebanon	Chekka	Water collected by plastic tubing until the 1960s	768	11	583
Bahrein		Drinking water	5	0.0	5
Indonesia	Ngobaran Beach, Java	Drinking water	2354	38	2354
Greece	Kiveri	Submarine spring dammed and used for irrigation	94	15	123
Peru	Surquillo	Drinking water	600	0.4	855
Mozambique	Quissico	Washing	0	0.0	138
Indonesia	East Lombok	Drinking water	691	4.9	1733
Australia	Pt. Willunga	Submarine springs important for local aboriginal culture	76	0.0	52

Table S7. Modeled coastal groundwater discharge for locations with reported impacts of groundwater discharge on coastal solute and nutrient budgets.

Reference	Country	Location	Reported impact of coastal groundwater discharge	Modeled CGD (m² a⁻¹)			Nitrogen application
				best	min.	max.	kg ha⁻¹
[65]	Portugal	Ria Formosa	Eutrophication	546	26	989	8
[79]	Mexico	Eastern Yucatan	Pollution of mangroves and coral reefs	92	0.1	308	0.2
[81]	Israel	Eilat	Eutrophication coral reef	49	0.2	62	1.0
[81]	U.S.A.	Key Largo	Eutrophication coral reef	394	0.2	2480	0.9
[82]	Australia	Moreton Bay	Carbon budget mangroves	233	0.03	818	21
[83]	U.S.A.	South Carolina	Nutrient budget salt marsh	177	0.2	315	2
[84]	Australia	Perth	Nutrient budget lagoon	160	11	181	22
[85]	U.S.A.	Tampa Bay	Algal blooms	766	0.01	2019	56

References

1. Toth, J. A theoretical analysis of groundwater flow in small drainage basins. *J. Geophys. Res.* **68**, 4795–4812 (1963).

2. Gleeson, T. & Manning, A. H. Regional groundwater flow in mountainous terrain: Three-dimensional simulations of topographic and hydrogeologic controls. *Water Resour. Res.* **44**, (2008).

3. Haitjema, H. M. & Mitchell-Bruker, S. Are Water Tables a Subdued Replica of the Topography? *Groundwater* **43**, 781–786 (2005).

4. Fan, Y. & Schaller, M. F. River basins as groundwater exporters and importers: Implications for water cycle and climate modeling. *J. Geophys. Res. Atmos.* **114**, (2009).

5. Lehner, B. & Grill, G. Global river hydrography and network routing: baseline data and new approaches to study the world's large river systems. *Hydrol. Process.* **27**, 2171–2186 (2013).

6. Wessel, P. & Smith, W. H. F. A Global, Self-consistent, Hierarchical, High-Resolution Shoreline Database. *J. Geophys. Res.* **101**, 8741–8743 (1996).

7. Gleeson, T., Moosdorf, N., Hartmann, J. & van Beek, L. P. H. A glimpse beneath earth's surface: GLobal HYdrogeology MaPS (GLHYMPS) of permeability and porosity. *Geophys. Res. Lett.* **41**, 1–8 (2014).

8. Hartmann, J. & Moosdorf, N. The new global lithological map database GLiM: A representation of rock properties at the Earth surface. *Geochemistry, Geophys. Geosystems* **13**, 1–37 (2012).

9. Gleeson, T. *et al.* Mapping permeability over the surface of the Earth. *Geophys. Res. Lett.* **38**, 1–6 (2011).

10. Fleury, P., Bakalowicz, M. & de Marsily, G. Submarine springs and coastal karst aquifers: A review. *J. Hydrol.* **339**, 79–92 (2007).

11. Appelo, C. A. J. & Postma, D. *Geochemistry, groundwater and pollution*. (A.A. Balkema publishers, 2006).

12. Bauer-Gottwein, P. *et al.* Review: The Yucatan Peninsula karst aquifer, Mexico. *Hydrogeol. J.* **19**, 507–524 (2011).

13. Ghasemizadeh, R. *et al.* Review: Groundwater flow and transport modeling of karst aquifers, with particular reference to the North Coast Limestone aquifer system of Puerto Rico. *Hydrogeol. J.* **20**, 1441–1461 (2012).

14. Panagopoulos, G. Application of MODFLOW for simulating groundwater flow in the Trifilia karst aquifer, Greece. *Environ. Earth Sci.* **67**, 1877–1889 (2012).

15. De Graaf, I. E. M., Sutanudjaja, E. H., Van Beek, L. P. H. & Bierkens, M. F. P. A high-resolution

global-scale groundwater model. *Hydrol. Earth Syst. Sci.* **19**, 823–837 (2015).

16. Döll, P. & Fiedler, K. Global-scale modeling of groundwater recharge. *Hydrol. Earth Syst. Sci.* **12**, 863–885 (2008).

17. Danielson, J. J. & Gesch, D. B. Global multi-resolution terrain elevation data 2010 (GMTED2010). *US Geol. Surv. Open File Rep* **1073**, 25 (2011).

18. Trabucco, A. & Zomer, R. J. Global aridity index (global-aridity) and global potential evapo-transpiration (global-PET) geospatial database. *CGIAR Consortium for Spatial Information* (2009).

19. Muis, S., Verlaan, M., Winsemius, H. C., Aerts, J. C. J. H. & Ward, P. J. A global reanalysis of storm surges and extreme sea levels. *Nat. Commun.* **7**, (2016).

20. Fan, Y., Li, H. & Miguez-Macho, G. Global patterns of groundwater table depth. *Science (80-.).* **339**, 940–943 (2013).

21. Gross, L., Bourgouin, L., Hale, A. J. & Muhlhaus, H.-B. Interface Modeling in Incompressible Media using Level Sets in Escript. *Phys. Earth Planet. Inter.* **163**, 23–34 (2007).

22. Poulet, T., Gross, L., Georgiev, D. & Cleverley, J. escript-RT: Reactive transport simulation in Python using escript. *Comput. \& Geosci.* **45**, 168–176 (2012).

23. Langevin, C. D., Thorne Jr., D. T., Dausman, A. M., Sukop, M. C. & Guo, W. *SEAWAT Version 4: A Computer Program for Simulation of Multi-Species Solute and Heat Transport*. (2008).

24. Voss, C. I. & Provost, A. M. *SUTRA, A model for saturated-unsaturated variable-density ground-water flow with solute or energy transport*. (2002).

25. Poulet, T. *et al.* Thermal-mechanical-hydrological-chemical simulations using escript, Abaqus and WinGibbs. in *Abstract for the GeoMod 2010 Conference, 27e29 September* (2010).

26. Hale, A. J. *et al.* Dynamics of slab tear faults: Insights from numerical modelling. *Tectonophysics* **483**, 58–70 (2010).

27. Ingebritsen, S. E., Sanford, W. E. & Neuzil, C. E. *Groundwater in geologic processes*. (Cambridge Univ Press, 2006).

28. Scheidegger, A. E. General theory of dispersion in porous media. *J. Geophys. Res.* **66**, 3273–3278 (1961).

29. Batzle, M. & Wang, Z. Seismic properties of pore fluids. *Geophysics* **57**, 1396–1408 (1992).

30. Ackerer, P. A new coupling algorithm for density-driven flow in porous media. *Geophys. Res. Lett.* **31**, L12506 (2004).

31. Diersch, H.-J. G. & Kolditz, O. Variable-density flow and transport in porous media: approaches and challenges. *Adv. Water Resour.* **25**, 899–944 (2002).

32. Glover, R. E. The pattern of fresh water flow in a coastal aquifer. *J. Geophys. Res.* **64**, 457–459 (1959).

33.   Batelaan, O. & De Smedt, F. SEEPAGE, a new MODFLOW DRAIN package. *Ground Water* **42**, 576–88 (2004).

34.   Gleeson, T., Befus, K. M., Jasechko, S., Luijendijk, E. & Cardenas, M. B. The global volume and distribution of modern groundwater. *Nat. Geosci.* **9**, 161–167 (2016).

35.   Jasechko, S. *et al.* Global aquifers dominated by fossil groundwaters but wells vulnerable to modern contamination. *Nat. Geosci.* **10**, 425–429 (2017).

36.   Courant, R., Friedrichs, K. & Lewy, H. Über die partiellen Differenzengleichungen der mathematischen Physik. *Math. Ann.* **100**, 32–74 (1928).

37.   Goswami, R. R. & Clement, T. P. Laboratory-scale investigation of saltwater intrusion dynamics. *Water Resour. Res.* **43**, n/a-n/a (2007).

38.   Bokuniewicz, H. J. Analytical Descriptions of Subaqueous Groundwater Seepage. *Estuaries* **15**, 458 (1992).

39.   Henry, H. R. Salt intrusion into fresh-water aquifers. *J. Geophys. Res.* **64**, 1911–1919 (1959).

40.   Simpson, M. J. & Clement, T. P. Theoretical analysis of the worthiness of Henry and Elder problems as benchmarks of density-dependent groundwater flow models. *Adv. Water Resour.* **26**, 17–31 (2003).

41.   Bresciani, E., Davy, P. & De Dreuzy, J. R. Is the Dupuit assumption suitable for predicting the groundwater seepage area in hillslopes? *Water Resour. Res.* **50**, 2394–2406 (2014).

42.   Gelhar, L. W., Welty, C. & Rehfeldt, K. R. A Critical Review of Data on Field-Scale Dispersion in Aquifers Lynn W. Gelhar, Claire Welty, Kenneth R. Rehfeldt. *Water Resour. Res.* **28**, 1955–1974 (1992).

43.   Oude Essink, G. H. P. Salt Water Intrusion in a Three-dimensional Groundwater System in The Netherlands: A Numerical Study. *Transp. Porous Media* **43**, 137–158 (2001).

44.   Luijendijk, E. & Gleeson, T. How well can we predict permeability in sedimentary basins? Deriving and evaluating porosity-permeability equations for noncemented sand and clay mixtures. *Geofluids* **15**, 67–83 (2015).

45.   Olsthoorn, T. Finite Difference Grounwater Modeling in Python. (2017). Available at: https://olsthoorn.readthedocs.io/en/latest/01_Numerical_grw_modeling.html#.

46.   Jones, E., Oliphant, T. & Peterson, P. Scipy: Open source scientific tools for Python. (2013).

47.   Panno, S. V, Kelly, W. R., Martinsek, A. T. & Hackley, K. C. Estimating Background and Threshold Nitrate Concentrations Using Probability Graphs. *Ground Water* **44**, 697–709 (2006).

48.   Mueller, D. K. & Helsel, D. R. *Nutrients in the Nation's Waters--Too Much of a Good Thing? U.S. Geological Survey Circular* **1136**, (1996).

49.   Kessler, T. J. & Harvey, C. F. The global flux of carbon dioxide into groundwater. *Geophys. Res.*

Lett. **28**, 279–282 (2001).

50. Tréguer, P. J. & De La Rocha, C. L. The world ocean silica cycle. *Ann. Rev. Mar. Sci.* **5**, 477–501 (2013).

51. Beck, A. J., Charette, M. A., Cochran, J. K., Gonneea, M. E. & Peucker-Ehrenbrink, B. Dissolved strontium in the subterranean estuary - Implications for the marine strontium isotope budget. *Geochim. Cosmochim. Acta* **117**, 33–52 (2013).

52. Ascott, M. J. *et al.* Global patterns of nitrate storage in the vadose zone. *Nat. Commun.* **8**, 1416 (2017).

53. Frings, P. J., Clymans, W., Fontorbe, G., Christina, L. & Conley, D. J. The continental Si cycle and its impact on the ocean Si isotope budget. *Chem. Geol.* **425**, 12–36 (2016).

54. Beusen, A. H. W., Slomp, C. P. & Bouwman, A. F. Global land–ocean linkage: direct inputs of nitrogen to coastal waters via submarine groundwater discharge. *Environ. Res. Lett.* **8**, 034035 (2013).

55. Cole, J. J. *et al.* Plumbing the global carbon cycle: integrating inland waters into the terrestrial carbon budget. *Ecosystems* **10**, 172–185 (2007).

56. Potter, P., Ramankutty, N., Bennett, E. M. & Donner, S. D. Characterizing the Spatial Patterns of Global Fertilizer Application and Manure Production. *Earth Interact.* **14**, 1–22 (2010).

57. Redding, J. E. *et al.* Link between sewage-derived nitrogen pollution and coral disease severity in Guam. *Mar. Pollut. Bull.* **73**, 57–63 (2013).

58. Alder, J. Putting the coast in the 'Sea Around Us'. *Sea Around Us Newsl.* **15**, 1–2 (2003).

59. Mcowen, C. J. *et al.* A global map of saltmarshes. *Biodivers. Data J.* **5**, e11764 (2017).

60. UNEP-WCMC, WorldFish Centre, WRI & TNC. Global distribution of warm-water coral reefs, compiled from multiple sources including the Millennium Coral Reef Mapping Project. Version 1.3. (2010).

61. Martin, J. B., Cable, J. E., Smith, C., Roy, M. & Cherrier, J. Magnitudes of submarine groundwater discharge from marine and terrestrial sources: Indian River Lagoon, Florida. *Water Resour. Res.* **43**, (2007).

62. Michael, H. A., Lubetsky, J. S. & Harvey, C. F. Characterizing submarine groundwater discharge: A seepage meter study in Waquoit Bay, Massachusetts. *Geophys. Res. Lett.* **30**, (2003).

63. Russoniello, C. J. *et al.* Geologic effects on groundwater salinity and discharge into an estuary. *J. Hydrol.* **498**, 1–12 (2013).

64. Taniguchi, M. *et al.* Submarine groundwater discharge from the Yellow River Delta to the Bohai Sea, China. *J. Geophys. Res. Ocean.* **113**, (2008).

65. Leote, C., Ibánhez, J. S. & Rocha, C. Submarine groundwater discharge as a nitrogen source to

the Ria Formosa studied with seepage me61ters. *Biogeochemistry* **88**, 185–194 (2008).

66. Hays, R. L. & Ullman, W. J. Direct determination of total and fresh groundwater discharge and nutrient loads from a sandy beachface at low tide (Cape Henlopen, Delaware). *Limnol. Oceanogr.* **52**, 240–247 (2007).

67. Niencheski, L. F. H., Windom, H. L., Moore, W. S. & Jahnke, R. A. Submarine groundwater discharge of nutrients to the ocean along a coastal lagoon barrier, Southern Brazil. *Mar. Chem.* **106**, 546–561 (2007).

68. Santos, I. R., Burnett, W. C., Chanton, J., Dimova, N. & Peterson, R. N. Land or ocean?: Assessing the driving forces of submarine groundwater discharge at a coastal site in the Gulf of Mexico. *J. Geophys. Res. Ocean.* **114**, (2009).

69. de Sieyes, N. R., Yamahara, K. M., Layton, B. a., Joyce, E. H. & Boehm, A. B. Submarine discharge of nutrient-enriched fresh groundwater at Stinson Beach, California is enhanced during neap tides. *Limnol. Oceanogr.* **53**, 1434–1445 (2008).

70. Spinelli, G. A. *et al.* Groundwater seepage into northern San Francisco Bay: Implications for dissolved metals budgets. *Water Resour. Res.* **38**, 12–19 (2002).

71. Strack, O. D. L. A single-potential solution for regional interface problems in coastal aquifers. *Water Resour. Res.* **12**, 1165–1174 (1976).

72. Vries, J. J. de & Simmers, I. Groundwater recharge: an overview of processes and challenges. *Hydrogeol. J.* **V10**, 5–17 (2002).

73. Scanlon, B. R., Healy, R. W. & Cook, P. G. Choosing appropriate techniques for quantifying groundwater recharge. *Hydrogeol. J.* **10**, 18–39 (2002).

74. Sawyer, A. H., David, C. H. & Famiglietti, J. S. Continental patterns of submarine groundwater discharge reveal coastal vulnerabilities. *Science (80-.).* **10**, 705–708 (2016).

75. Younger, P. L. Submarine groundwater discharge. *Nature* **382**, 121–122 (1996).

76. Burnett, W. C. *et al.* Quantifying submarine groundwater discharge in the coastal zone via multiple methods. *Sci. Total Environ.* **367**, 498–543 (2006).

77. Stewart, B. T., Santos, I. R., Tait, D. R., Macklin, P. A. & Maher, D. T. Submarine groundwater discharge and associated fluxes of alkalinity and dissolved carbon into Moreton Bay (Australia) estimated via radium isotopes. *Mar. Chem.* **174**, 1–12 (2015).

78. Taniguchi, M., Burnett, W. C., Cable, J. E. & Turner, J. V. Investigation of submarine groundwater discharge. *Hydrol. Process.* **16**, 2115–2129 (2002).

79. Hernández-Terrones, L. *et al.* Groundwater pollution in a karstic region (NE Yucatan): Baseline nutrient content and flux to coastal ecosystems. *Water. Air. Soil Pollut.* **218**, 517–528 (2011).

80. Moosdorf, N. & Oehler, T. Societal use of fresh submarine groundwater discharge: An overlooked water resource. *Earth-Science Rev.* **171**, 338–348 (2017).

81.   Paytan, A. *et al.* Submarine groundwater discharge: An important source of new inorganic nitrogen to coral reef ecosystems. *Limnol. Oceanogr.* **51**, 343–348 (2006).

82.   Maher, D. T., Santos, I. R., Golsby-Smith, L., Gleeson, J. & Eyre, B. D. Groundwater-derived dissolved inorganic and organic carbon exports from a mangrove tidal creek: The missing mangrove carbon sink? *Limnol. Oceanogr.* **58**, 475–488 (2013).

83.   Krest, J. M., Moore, W. S., Gardner, L. R. & Morris, J. T. Marsh nutrient export supplied by groundwater discharge: Evidence from radium measurements. *Global Biogeochem. Cycles* **14**, 167–176 (2000).

84.   Johannes, R. E. & Hearn, C. J. The effect of submarine groundwater discharge on nutrient and salinity regimes in a coastal lagoon off Perth, Western Australia. *Estuar. Coast. Shelf Sci.* **21**, 789–800 (1985).

85.   Hu, C., Muller-Karger, F. E. & Swarzenski, P. W. Hurricanes, submarine groundwater discharge, and Florida's red tides. *Geophys. Res. Lett.* **33**, (2006).